2557-2-F
FINAL REPORT

A PRELIMINARY STUDY OF VISIBILITY ON THE HIGHWAY IN FOG

Benjamin S. Pritchard

H. Richard Blackwell

Vision Research Laboratories

July 1957

ENGINEERING RESEARCH INSTITUTE
The University of Michigan
Ann Arbor, Michigan

TABLE OF CONTENTS

TABLE OF CONTENTS (Con't.)

LIST OF FIGURES

LIST OF FIGURES (con't.)

LIST OF TABLES

SUMMARY

A program of studies is reported, which was intended to lay the foundation for an understanding of the problem of improving visibility on the highway in fog.

Our major effort was devoted to measurements of the precise optical properties of natural (and artificial fogs), including transmittance and the polar distribution of light scatter. The theoretical background of measurements of these physical characteristics of the atmosphere is indicated. Two new measurement devices, the Recording Polar Nephelometer and the Portable Transmissometer are described. Polar Scattering Diagrams are presented for a number of real fogs, and for several types of artificial fog intended for use in scale-model simulation of the highway problem in fog. The Polar Scatter Diagrams reveal major departures from theoretical expectations, which have important relevance to the highway problem. Happily, it was found that artificial fogs produced from water droplets do provide an adequate simulation of real fogs.

Sample calculations have been made to illustrate the use of Polar Scattering Diagrams in the analysis and evaluation of practical problems of visibility through fog. The calculational technique utilizes new data on the polar distribution of light scatter and previously reported data on human vision.

Two general methods are described for improving the design of street lights for use in fog. One method involves restricting the wide beam of street lights to permit principally "down-lighting" of the roadway. The other method involves the use of linearly polarized street lights and an analyzer of opposite polarization. These methods were suggested by the form of the Polar Scattering Diagrams. Preliminary evaluations of these methods in a scale-model simulator were quite favorable, indicating that further study of these ideas should be fruitful.

The scale-model simulator used to evaluate these preliminary ideas appears to be useful for evaluating a number of possible changes in street lights, vehicle headlamps and taillights, and roadway markers. It is recommended that this type simulator be used extensively in further studies of the problem of improving visibility on the highway in fog.

I. INTRODUCTION

The present report summarizes the experimental studies conducted under Engineering Research Institute Project 2557, established in terms of Grant #47B from the Illuminating Engineering Research Institute. These studies were concerned with various aspects of the problem of improving visibility on the highway in fog.

The major effort on Project 2557 was devoted to measurements of the optical properties of fog. These measurements have been used both to perform computational evaluations of various general methods of lighting the highway in fog, and to evaluate the feasibility of producing artificial fog with the optical properties of natural fog. A small effort was devoted to construction of a scale-model simulator, involving a roadway, automobiles, roadway markers, and street lights. Fog with optical properties simulating natural fog was introduced into the simulator at an appropriate scaled density. Qualitative observations have been made in the scale-model simulator which confirmed expectations based upon previous analyses of the problem.

The program of research conducted under Project 2557 was closely coordinated with a program conducted at the Pennsylvania State University by Charles R. Marsh. Prof. Marsh initially conducted full-scale field tests of various methods of lighting the highway during fog. Because of the difficulties encountered in finding fog at convenient locations, Marsh then explored the development of artificial fog. Measurements made under the Michigan program guided Prof. Marsh to the development of a satisfactory artificial fog.

The two research programs were described in some detail at a "Visibility Through Fog Demonstration" conducted at the Pennsylvania State University on June 28, 1957. The present report is intended to present the scientific substantiation for the various results reported at this demonstration.

II. GENERAL ASPECTS OF THE PROBLEM OF VISIBILITY THROUGH FOG

Extensive studies of human vision conducted in these laboratories since 1946 have established the primary physical variables which influence visibility through fog. These are (a) the over-all luminance of the background against which objects are seen; and (b) the luminance contrast between objects and their backgrounds. The higher the object contrast for fixed background luminance, the smaller will be the angular subtense of a target which is just visible, and hence the farther will the object be seen. Precise quantitative relations among these variables are shown in Figure 1. These data are a portion of a previous report (Ref. 1).

The quantitative values of general background luminance and object contrast to be expected on the highway in fog depend in a complex manner upon the precise distributions of illumination used to improve visibility, and the optical properties of the atmosphere. Some conception of the problem may be gained from Figure 2. Here we have represented a headlamp light beam and a light beam from an overhead street light. These light beams illuminate the truck and roadway, and also the atmosphere intervening between the sources of light and these objects. Some light rays reach the truck and roadway through the fog. Other light rays are absorbed by particles in the atmosphere. Still other light rays are scattered, i.e., redirected, by the atmosphere. The vector arrows indicate the directions and magnitudes of light scattered by fog particles in the atmosphere. This scattering first modifies the pattern of illumination which reaches the truck and the roadway, both due to light rays which are redirected and therefore miss the truck and roadway, and due to light rays which strike the truck and roadway because they are redirected. Scattering further modifies the pattern of luminances of the truck and roadway by redirecting light rays reflected from these objects.

The scene presented to the driver contains two other classes of luminance. First, self-luminous objects, such as the truck taillight are seen with a luminance dependent primarily upon the light rays which come to the driver's eyes without scatter by the atmosphere. Secondly, the atmosphere is seen as a light-veil superimposed between the driver's eyes and various objects. The luminance of the light-veil depends in part upon the illuminance striking each fog particle and in part upon the magnitude of the scattering vector in the direction of the driver's eye. In fact, the luminance of the veil in a particular direction represents a kind of sum of the effects of all the particles along the line-of-sight in that direction. The general effect of the light-veil is to reduce the luminance contrast of objects viewed through it, to an extent dependent upon the luminance of the veil compared with the luminances of the objects and their background.

In our initial analysis of the fog visibility problem, we became convinced that we could gain considerable insight into the problem if we could specify the luminances of object-backgrounds and the luminance contrast of objects against these backgrounds. Sufficient knowledge was available on the characteristics of light beams produced by headlamps, overhead street lights and taillights. Our major lack of information concerned the precise characteristics of the scattering vectors of foggy atmospheres. Accordingly, our major efforts on this Project were directed at measuring the light-scattering characteristics of fog in detail. The theoretical background of this problem, our instrumentation, and our research data are reported in Section II following. The following section presents computational analyses of sample fog visibility problems.

III. STUDIES OF OPTICAL PROPERTIES OF THE ATMOSPHERE

A. Equations and Theory

The symbols used here are those used by Middleton (Ref. 2), and by Perrin (Ref. 3).

The transmittance (T) of an air path is the ratio of the final flux in a light beam (P) to the initial flux (P_o):

$$T = \frac{P}{P_o} \tag{1}$$

For an homogeneous path of length D, the transmittance is exponentially related to the distance:

$$T = e^{-\sigma D} \tag{2}$$

where σ is the attenuation coefficient. The meteorological range, V, is that distance for which the transmittance falls to 2%. Consequently,

$$V = \frac{3.912}{\sigma} \tag{3}$$

Because attenuation occurs as a result of scattering and absorption, σ may be expressed as the sum of a scattering coefficient (b) and an absorption coefficient (k). Thus,

$$\sigma = b+k \tag{4}$$

The volume scattering index (β') is defined by the following equation:

$$dJ = \beta' H \, dv \tag{5}$$

where dv is the volume of an element of sample illuminated by parallel monochromatic light of irradiance H, and dJ is the radiant intensity (i.e., flux per steradian) of the energy scattered in a particular direction by that element. β', and consequently dJ, are functions of the angle (Φ) between the directions of propagation of the incident and scattered light.

As the sum of the light scattered in all directions must equal the total amount of light scattered from the beam, b and β' are related by the following equation:

$$b = 2\pi \int_0^{\pi} \beta'_{UU} \sin \Phi \, d\Phi \tag{6}$$

where β'_{UU} is the value of β' measured with unpolarized incident light and unpolarized receiver.

The preceding equations are often written in photometric symbols:

$$T = \frac{F}{F_0} \tag{7}$$

$$dI = \beta' E \, dv \tag{8}$$

Regardless of the notation employed, it must be realized that T, σ, b, k, and β' are functions of wavelength, and that large errors in scattering and attenuation calculations can result if measurements are made with white light and a broad-band receiver.

Since the polarization of the incident light is well preserved during direct transmission through the atmosphere, it is not customary to consider polarization in the transmission equations. In scattering, however, polarization is preserved in some situations and greatly altered in others, depending in a complex way upon the nature of the sample, the wavelength, the scattering angle, and the incident polarization. These properties may be specified in an orderly and convenient manner by stating β' for each value of Φ and λ in terms of a Mueller matrix (Ref. 4, 5) which relates the Stokes parameters (Ref. 6) of the scattered light to the Stokes parameters of the incident light.

The general form of the Mueller matrix contains sixteen independent coefficients. Perrin (Ref. 3) has shown that if a scattering medium is both isotropic and free of optical activity, the scattering matrix contains only six independent coefficients and may be written in the form:

$$\begin{vmatrix} a_1 & b_1 & 0 & 0 \\ b_1 & a_2 & 0 & 0 \\ 0 & 0 & a_3 & b_2 \\ 0 & 0 & -b_2 & a_4 \end{vmatrix} \tag{9}$$

or, in normalized form:

$$a_1 \begin{vmatrix} 1.00 & b_1' & 0 & 0 \\ b_1' & a_2' & 0 & 0 \\ 0 & 0 & a_3' & b_2' \\ 0 & 0 & -b_2' & a_4' \end{vmatrix} \tag{10}$$

where:

$$a_2' = \frac{a_2}{a_1} \tag{11}$$

$$a_3' = \frac{a_3}{a_1} \tag{12}$$

$$a_4' = \frac{a_4}{a_1} \tag{13}$$

$$b_1' = \frac{b_1}{a_1} \tag{14}$$

$$b_2' = \frac{b_2}{a_1} \tag{15}$$

This applies to any natural aerosol except possibly rain or snow, where non-random movement of the particles with respect to the surrounding air may destroy the isotropy.

In an unpublished communication, Dr. R. Clark Jones has pointed out that:

> "Actually, the matrix will still have the above form under slightly less restrictive conditions than complete isotropy. If (1) the medium is symmetrical in the sense that the transmittance is unchanged if the light path is reversed and polarizer and analyzer are interchanged, and if (2) the medium is such that horizontally or vertically polarized light is scattered as horizontally or vertically partially polarized light, then the matrix will still have the above form [for a horizontal scattering plane].
>
> "Condition (1) certainly holds for any natural aerosol and condition (2) will hold even if the particles consist of needles or

plates [or distorted droplets] provided that the angular distribution is such that there is symmetry about a vertical axis or a horizontal plane through the sample."

Perrin has also shown that in direct forward scatter ($\Phi = 0$) the matrix reduces to:

$$\begin{vmatrix} a_1^o & 0 & 0 & 0 \\ 0 & a_2^o & 0 & 0 \\ 0 & 0 & a_2^o & 0 \\ 0 & 0 & 0 & a_4^o \end{vmatrix} \tag{16}$$

and in direct back scatter ($\Phi = \pi$) to:

$$\begin{vmatrix} a_1^\pi & 0 & 0 & 0 \\ 0 & a_2^\pi & 0 & 0 \\ 0 & 0 & -a_2^\pi & 0 \\ 0 & 0 & 0 & a_4^\pi \end{vmatrix} \tag{17}$$

In fog, the droplets will assume a spherical shape as a result of the strong effect of surface tension at small radii. Perrin has shown that in this case:

$$a_1 = a_2 \tag{18}$$

$$a_3 = a_4 \tag{19}$$

Consequently the forward scatter matrix for fog is the same as that for a non-depolarizing filter:

$$\begin{vmatrix} a_1^o & 0 & 0 & 0 \\ 0 & a_1^o & 0 & 0 \\ 0 & 0 & a_1^o & 0 \\ 0 & 0 & 0 & a_1^o \end{vmatrix} \tag{20}$$

and the direct back scatter fog matrix should be the same as that of a non-depolarizing reflector:

$$\begin{vmatrix} a_1^{\pi} & 0 & 0 & 0 \\ 0 & a_1^{\pi} & 0 & 0 \\ 0 & 0 & -a_1^{\pi} & 0 \\ 0 & 0 & 0 & -a_1^{\pi} \end{vmatrix} \tag{21}$$

The coefficients of the scattering matrix can be determined from measurements of β' made with various combinations of six basic types of linear and circular polarizers denoted by the symbols H, V, D, d, R, and L. H and V indicate that the electric vector is horizontal and vertical, respectively. D and d indicate that the electric vector is inclined at 45 degrees to the horizontal, pointing toward the upper right and toward the upper left, respectively, looking in the direction of propagation. R and L indicate that the vector is rotating clockwise and counter-clockwise, respectively, again looking in the direction of propagation. If the scattering plane is other than horizontal, the definitions of H, V, D, and d must be interpreted accordingly, with the scattering plane instead of the horizon as reference. For the polarizer, the symbols indicate the state of polarization of the transmitted light, but for the analyzer they indicate which component of the incident light is accepted.

One set of measurements which can be employed is HH, VV, HV, DD, RR, and DR, where the first letter stands for the polarizer and the second for the analyzer. From these measurements the general scattering matrix coefficients may be computed:

$$a_1 = 1/2\ \beta'_{HH} + 1/2\ \beta'_{VV} + \beta'_{HV} = \beta'_{UU} \tag{22}$$

$$a_2 = 1/2\ \beta'_{HH} + 1/2\ \beta'_{VV} - \beta'_{HV} \tag{23}$$

$$a_3 = 2\ \beta'_{DD} - a_1 \tag{24}$$

$$a_4 = 2\ \beta'_{RR} - a_1 \tag{25}$$

$$b_1 = 1/2\ \beta'_{HH} - 1/2\ \beta'_{VV} \tag{26}$$

$$b_2 = a_1 - 2\ \beta'_{DR} \tag{27}$$

The other thirty combinations of the six basic types of linear and circular polarizers are either equal to or deriveable from the measured six:

$$\beta'_{HH} = 1/2\ (a_1 + a_2) + b_1 \tag{28}$$

$$\beta'_{VV} = 1/2\ (a_1 + a_2) - b_1 \tag{29}$$

$$\beta'_{HV} = \beta'_{VH} = 1/2\ (a_1 - a_2) \tag{30}$$

$$\beta'_{DD} = \beta'_{dd} = 1/2\ (a_1 + a_3) \tag{31}$$

$$\beta'_{Dd} = \beta'_{dD} = 1/2\ (a_1 - a_3) \tag{32}$$

$$\beta'_{RR} = \beta'_{LL} = 1/2\ (a_1 + a_4) \tag{33}$$

$$\beta'_{RL} = \beta'_{LR} = 1/2\ (a_1 - a_4) \tag{34}$$

$$\beta'_{RD} = \beta'_{dR} = \beta'_{Ld} = \beta'_{DL} = 1/2\ (a_1 + b_2) \tag{35}$$

$$\beta'_{DR} = \beta'_{Rd} = \beta'_{LD} = \beta'_{dL} = 1/2\ (a_1 - b_2) \tag{36}$$

$$\beta'_{HD} = \beta'_{Hd} = \beta'_{HR} = \beta'_{HL} = \beta'_{DH} = \beta'_{dH} = \beta'_{RH} = \beta'_{LH} = 1/2\ (a_1 + b_1) \tag{37}$$

$$\beta'_{VD} = \beta'_{Vd} = \beta'_{VR} = \beta'_{VL} = \beta'_{DV} = \beta'_{dV} = \beta'_{RV} = \beta'_{LV} = 1/2\ (a_1 - b_1) \tag{38}$$

B. The Recording Polar Nephelometer

The Recording Polar Nephelometer measures the scattering index β'. The scattering angle Φ is the independent variable, with polarization and wavelength usually taken as parameters.

In 1945, Waldram (Ref. 6) described an atmospheric polar nephelometer which was built in England during World War II. Considering the relative simplicity of design and the adverse conditions under which it was used, the results achieved are remarkable. This device contained an incandescent lamp and a reflector to form a horizontal light beam. A visual comparison photometer was mounted on a pivoted arm in such a way that the luminance of a portion of the light beam could be measured from various angles in a horizontal plane.

Our Polar Nephelometer is similar in many respects to the Waldram instrument. It consists of a circular base four feet in diameter upon which is fastened a projector in a fixed position (Fig. 3). A photo-

multiplier photometer is mounted on an arm pivoted at the center of the base. A light trap absorbs the projected beam, and a second light trap opposite the photomultiplier provides a black background for viewing the beam. As the arm rotates, the output of the photomultiplier is plotted on a strip chart recorder.

The region defined by the intersection of the projector and receiver beams is the "sample space." As the volume of the sample space changes with the viewing angle, some method of correction is necessary in order to comply with equation (5). Waldram's instrument employed an aperture plate which altered the width of the projector beam as the arm rotated. In the present instrument, the correction to constant volume is done computationally during data reduction.

Figure 4 shows the optical system of the Polar Nephelometer. A tightly coiled tungsten filament is imaged by an aspheric condensor at a rectangular field aperture; this is then imaged at the center of the instrument by the objective lens. A lens near the field aperture images the condensor in the plane of the objective. Angular resolving power is improved by a vertical rectangular aperture at the objective lens. The partially polarized light emitted by the lamp is, in effect, depolarized by a calcite multiple-wave retardation plate (Ref. 8). A sheet polarizer is usually employed in the position shown. The chopper consists of a vertical cylinder from which a section has been removed. As the cylinder rotates about its axis, it interrupts the light at the rate of 13 cycles-per-second.

The lens and aperture system of the receiver is identical to that of the projector, and a 1P21 photomultiplier is the sensitive element. Space is provided to insert neutral filters, color filters, and polarizers.

The light traps (Fig. 5) are made of polished plates of black glass. Most of the light entering the trap is absorbed by the first glass plate. The specular reflection is directed further into the trap, where it is absorbed during many additional reflections. Hence the only light leaving the trap is from non-specular reflection at the first surface. Black glass was chosen because it has an unusually low non-specular reflectance of only 6×10^{-6} for a selected, clean, dust-free surface. Since the critical first surface faces downward, dust accumulates slowly, and the trap performs satisfactorily without attention for long periods of time.

1. Design Considerations

Portability, simplicity, and ease of operation are requisites of an instrument for all-weather field measurements. Due to the variability of atmospheric conditions, measurements should be performed as rapidly as possible. Since small-angle forward and backward scattering are important for practical as well as theoretical reasons, the arm should be capable of swinging as far as possible in both directions. The angular resolving power should be as high as possible. All of these features must be

compromised, however, to achieve adequate sensitivity.

For a system in which the source and photocathode are imaged at the sample, the flux received by the photocathode is approximately equal to:

$$F = \beta' v \, B_S \, T_P \, T_R \, \frac{A_P \, A_R}{D^4} \qquad (39)$$

where v is the volume of the sample space, B_S is the luminance of the source (in flux per steradian per unit area), T_P and T_R are the transmittances of the lenses and filters in the projector and receiver, A_P and A_R are the areas of the apertures on the objective lenses of the projector and receiver, and D is the distance from each objective lens to the sample. From this equation it is evident that if all linear dimensions of the instrument were multiplied by some number, n, the flux would be increased by n^3. Therefore the instrument must be large if high sensitivity is required.

It is also evident from equation (39) that increasing v, A_P, and A_R, or decreasing D, improves the sensitivity; but each of these changes also reduces angular resolving power by increasing the spread of the rays in the projector and receiver beams. Further analysis has shown that the best compromise between sensitivity and resolving power results when the field and objective apertures are higher than they are wide, and when each beam is approximately the same size at the sample as at the objective lens. Sensitivity and resolving power may be interchanged by substituting various apertures. Three sets of apertures have been constructed which have the following characteristics:

APERTURE SET	APPROXIMATE RESOLUTION	RELATIVE SENSITIVITY
A	2°	1
B	5°	39
C	7°	185

A block diagram of the entire system is shown in Fig. 6. It was necessary to employ a chopped light system to discriminate between natural light and projector light because a cover which excluded daylight also altered the scattering properties of the atmospheric sample. The 13 cycle signal from the photomultiplier passes through a cathode follower, preamplifier, and Perkin Elmer 13 cycle amplifier. The signal is then rectified synchronously with the light chopper, and the resulting D.C. voltage actuates a Speedomax recorder. The recorder paper drive and the receiver arm are both driven by synchronous motors so that a known relation exists between chart motion and arm movement.

2. Calibration

The instrument is calibrated in absolute quantities by comparing the intensity of the light scattered by the atmosphere with the intensity from a standard. A new method of comparison has been developed which does not require any assumptions about the volume of the sample space, or uniformity of illumination or sensitivity. Consequently, it is applicable to any polar nephelometer optical system.

The standard is a diffusing plastic screen of measured reflectance and transmittance. Since the plastic is only 0.004 inches thick, the internal spreading of the light is negligible. This screen is placed in the sample space as shown in Figure 4 and moved in a direction perpendicular to the plane of the screen so that each pair of rays common to the projector and receiver beams is intercepted during its travel. The intensity of the light reflected or transmitted by the screen is recorded as it moves, and the integral thus obtained is compared with the intensity of the light scattered by an atmospheric sample. A proof of this method follows.

Consider a rectangular coordinate system oriented such that the plane xy is parallel to the scattering plane, and the plane yz is parallel to the plane of the diffusing screen. Direction x is then the direction of motion of the screen. If the screen is at position x, the illumination produced by the projector at point P(x, y, z) on the screen is E(x, y, z) cos γ', where γ' is the angle of incidence of the projector beam. The luminance B_c at this point, in the direction of the receiver, is:

$$B_c = \frac{R\ E \cos \gamma'}{\pi} \tag{40}$$

where R is the reflectance of the plastic under those conditions. For calibration at forward scattering angles, the screen is used in transmission and T replaces R in the above equation.

An element of area, dA, about P will have an intensity dI_c in the direction of the receiver:

$$dI_c = B_c \cos \gamma'' \, dA \tag{41}$$

where γ'' is the angle between the normal to the screen and the receiver axis. The amount of flux (dF_c) reaching the photocathode will be linearly related to the intensity by some factor C_1:

$$dF_c = C_1 \, dI_c \tag{42}$$

C_1 will be zero for P outside the receiver beam, and will, in general,

assume a different value for each point P. Assuming a linear transducer and amplifier, this flux will produce a scale reading dW_c on the recorder:

$$d\,W_c = C_2\,dF_c \tag{43}$$

C_2 takes into account the sensitivity of the photomultiplier, amplifiers, and recorder. In general, it will be a function of x, y, and z since each point P illuminates a different portion of a photocathode having nonuniform sensitivity. From equations (40 through 43):

$$d\,W_c = \frac{1}{\pi}\,R\cos\gamma'\cos\gamma''\,C_1\,C_2\,E\,dA \tag{44}$$

Integrating over the illuminated area yields:

$$W_c = \frac{R\cos\gamma'\cos\gamma''}{\pi}\iint_A C_1\,C_2\,E\,dA \tag{45}$$

If this is integrated again with respect to x, the following result is obtained:

$$\int_x W_c\,dx = \frac{R\cos\gamma'\cos\gamma''}{\pi}\int_x\iint_A C_1\,C_2\,E\,dAdx \tag{46}$$

Since dAdx = dv, this can be written:

$$\int_x W_c\,dx = \frac{R\cos\gamma'\cos\gamma''}{\pi}\iiint_v C_1\,C_2\,E\,dv \tag{47}$$

The plastic diffusing screen is removed when measuring an atmospheric sample. The illumination normal to the beam is again $E(x, y, z)$ at a point $P(x, y, z)$. An element of volume about P has an intensity dI_a, at an angle from the incident beam, given by equation (8):

$$dI_a = \beta'(\phi)\,E\,dv \tag{48}$$

The subscript "a" denotes an atmospheric sample. Since the same optical system is used during calibration and measurement, the same constants apply, and the flux at the photocathode is:

$$dF_a = C_1\,dI_a \tag{49}$$

This results in a recorder deflection:

$$d W_a = C_2 \, d F_a \tag{50}$$

Combining equations (48), (49), and (50):

$$d W = C_1 \, C_2 \, E \, \beta' \, dv \, . \tag{51}$$

Integration yields:

$$W_a = \beta' \iiint_v C_1 \, C_2 \, E \, dv \, . \tag{52}$$

β' has been removed from the integral because it is essentially constant over the small range of angles accepted at each arm position.

The final result is obtained by dividing equation (52) by equation (47):

$$\beta' = \frac{R \cos \gamma' \cos \gamma''}{\pi} \, \frac{W_a}{\int W_c \, dx} \tag{53}$$

or

$$\beta' = K \, W_a \tag{54}$$

where K, the calibration factor of the instrument, is defined by:

$$K = \frac{R \cos \gamma' \cos \gamma''}{\pi \int W_c \, dx} \, . \tag{55}$$

The value of $\int W_c \, dx$ is found by recording the signal as the calibration diffuser is moved through the sample space. If the recorder paper moves at the same rate as the diffusing screen, the area under the recorded curve is the desired integral.

It is necessary to repeat the calibration at a sufficiently large number of arm positions (or values of Φ) to define the curve of K versus Φ. This curve may be approximated by assuming that E, C_1 and C_2 are constant throughout the sample space. Equation (47) then reduces to:

$$\int W_c \, dx = \frac{1}{\pi} R \cos \gamma' \cos \gamma'' C_1 C_2 E v \, . \tag{56}$$

Substituting this into equation (55) yields:

$$K = \frac{1}{C_1 C_2 E v} \tag{57}$$

If the beams were collimated, v would be inversely proportional to sin Φ and, under the preceding assumptions, K would be directly proportional to sin Φ. In practice it has been found that K closely follows the sine function except at extreme angles.

To measure the appropriate values of R and T to be used in equation (55), the nephelometer is converted, in effect, into a goniophotometer. A diffusing plate is placed at the objective lens of the projector so that the plastic screen being measured is uniformly illuminated across its entire surface. With this arrangement, readings are taken for every combination of angle of incidence, angle of transmission and reflection, polarization, and color in which the screen is to be used. To convert from these relative readings to absolute reflectances, a primary reflectance standard is employed.

Before describing the standard, it is necessary to define some terms. The first is the unpolarized reflectance R_{UU} of a diffusing surface:

$$R_{UU} = \pi \frac{B_U}{E_U} \, , \tag{58}$$

where B_U is the luminance (flux per steradian per unit area) in a specified direction. B_U includes all types of polarization reflected by the surface, as measured by a photometer which is not polarization-sensitive. E_U is the unpolarized illuminance on the surface (flux per unit area) from a specified direction.

Correspondingly,

$$\beta'_{UU} = \frac{dI_U}{E_U \, dv} \tag{59}$$

where E_U is unpolarized and I_U includes all polarization components of the light scattered by the sample.

The polarized reflectance, R_{PP}, of a diffusing surface is:

$$R_{PP} = \pi \frac{B_P}{E_P} \tag{60}$$

Here the surface is illuminated from a specified direction by elliptically polarized light of illuminance E_p and wavelength λ. "Elliptical" is used here in the general sense, including linear and circular. B_p is a specified elliptically polarized component of the luminance of the surface.

Correspondingly,

$$\beta'_{PP} = \frac{dI_p}{E_p\, dv} \tag{61}$$

where E_p is the elliptically polarized illuminance, and dI_p is one polarized component of the scattered light.

A perfect diffuse reflector is defined as one which meets the following requirements:

(a) All incident light is reflected by the surface.
(b) The luminance of the surface is equal in all directions.
(c) The reflected light is unpolarized in all directions regardless of the polarization of the incident light.

The Mueller matrix of a perfect diffuse reflector is therefore:

$$\begin{vmatrix} 1 & 0 & 0 & 0 \\ 0 & 0 & 0 & 0 \\ 0 & 0 & 0 & 0 \\ 0 & 0 & 0 & 0 \end{vmatrix} \tag{62}$$

for all directions. This leads to an unpolarized reflectance of 1.0 and a polarized reflectance of 0.5, also independent of angle.

A smoked magnesium oxide surface nearly meets specifications (a) and (b) above, but it only partially depolarizes. For angles near the normal, the matrix of an MgO plate was found experimentally to be:

$$\begin{vmatrix} 0.98 & 0 & 0 & 0 \\ 0 & 0.10 & 0 & 0 \\ 0 & 0 & -0.10 & 0 \\ 0 & 0 & 0 & -0.03 \end{vmatrix} \tag{63}$$

A depolarizer consisting of two large crystals of ammonium dihydrogen phosphate* is used to complete the depolarization of the light reflected from the magnesium oxide surface. This effectively depolarizes a light beam regardless of the orientation of the depolarizer, provided only that the spectrum is continuous in an interval of at least several millimicrons.

The polarized reflectance of the combination of magnesium oxide and depolarizer is thus the product of the unpolarized reflectance of the oxide (0.98), the transmittance of the depolarizer (0.89 for green light), and the polarized reflectance of a perfect diffuse reflector (0.5). After this two-element primary standard of polarized reflectance has been used to standardize the goniophotometric measurements of the reflectance and transmittance of the plastic, the values can then be substituted into equation (55) to complete the calibration.

The calibration procedure just described is time-consuming and difficult; consequently, it is performed infrequently and only in the laboratory. In the field, changes in lamp output or system sensitivity are monitored by periodically inserting an opal plate into the sample space under specified and repeatable conditions.

C. The Portable Transmissometer

The Portable Transmissometer was designed to be readily transported and easily set up in a new location. The accuracy of determination of the extinction coefficient was required to be ± 5% under all conditions. Therefore, it was necessary to reduce stray light and other sources of error to a minimum. The accuracy requirement also demanded that the measured air path be variable depending upon atmospheric conditions.

These requirements are met by the instrument shown in Fig. 7. It consists essentially of two units, a projector and a receiver, each mounted on a surveyor's transit and tripod. The telescope and vernier controls provide a convenient means for precise field alignment of the two units. Power for the projector is furnished by a 12 volt storage battery. Lamp current is manually regulated with a precision of ± 0.05% with the aid of a null-balance comparison-circuit. The output of the receiver may be measured by a modified American Instrument Company photometer or by a battery-powered photometer.

1. Projector

The optical system of the projector is shown in Fig. 8. The salient feature of this system is a uniform distribution of intensity within a sharply defined beam, one half degree in diameter. This is achieved by filling the objective lens with an image of the lamp filament and forming an image, at the desired range, of an aperture which

*Available from Baird-Atomic, Inc.

is nearly conjugate to the condensor lens. As a result of filament image magnification produced by the relay lenses, a beam intensity of 13,000 candles is derived from a small 6 volt lamp of only 36 candles.

2. Receiver

As in the Polar Nephelometer, the principle of reciprocity shows that, for optimum performance, the distribution of sensitivity in the receiver should be the same as the intensity distribution of the projector. Consequently the optical systems of the two Transmissometer units are identical. In the receiver, a 1P21 photomultiplier is employed, and space is provided for color filters, neutral filters and polarizers. As the directional sensitivity of the photomultiplier is increased by the lenses of the receiver to the same extent that the lamp intensity is magnified in the projector, the two units may be separated by large distances.

The sensitivity of the receiver is monitored by frequently placing an extremely stable light source over the objective lens. The source, which has been described, (Ref. 9) consists of a phosphor activated by radioactive strontium.

3. Operation and Calibration

For use in fog, there are two calibration methods available. One is simply to divide the meter reading when the fog is present by that when the air is clear between projector and receiver. The other method is to employ two different separations, D_1 and D_2, both in fog. Both must be greater than 100 feet, the distance below which the inverse square law does not hold for this instrument. The transmittance of the path difference, $D_2 - D_1$, is then:

$$T_{2-1} = \frac{w_2 \, t_1 \, D_2^2}{w_1 \, t_2 \, D_1^2} \tag{64}$$

where t_1 and t_2 are the transmittances of carefully calibrated neutral filters employed to prevent overloading the photomultiplier. The attenuation coefficient is then:

$$\sigma = \frac{-\ln T_{2-1}}{D_2 - D_1} \tag{65}$$

In dense fog, the separation should be 100 feet or less, while in lighter fogs, a separation of several hundred feet results in higher accuracy.

4. Small Angle Scattering Measurements

A second use for the Portable Transmissometer is the measurement of small angle forward scatter. For this purpose, the two units are set up ten feet apart and pointed directly at each other. Each transit is then turned through half the desired scattering angle so that the beams intersect midway between the two instruments. Calibration is performed with a diffusing screen as in the Polar Nephelometer with the following simplification. For small values of Φ, the value of $\int W_c\, dx$ is inversely proportional to Φ. Therefore, the value of the integral need be obtained at only one value of $(\Phi = \Phi_c)$. Equation (5) can then be modified to

$$\beta' = \frac{T\, W_m}{\Phi_c\, \pi \int W_c\, dx} \qquad (66)$$

This method of measuring small angle scatter is unnecessarily time-consuming. Hence an attachment is being constructed for the Polar Nephelometer which will extend its measurement range to $2° < \Phi < 178°$.

5. Error Analysis

There are many sources of error which affect the accuracy of measurement of the attenuation coefficient. Those which are of principal concern in fog are: (a) small angle light-scatter which is accepted by the receiver; and (b) ordinary photometric errors such as changes in projector output, changes in receiver sensitivity, spectral effects, etc.

The error due to scattered light entering the receiver has been studied by several authors (Ref. 2, 10, 11). For the particular conditions imposed by this instrument, the fractional error in transmittance resulting from small angle forward scatter is:

$$\epsilon_s\,(T_{1\text{-}2}) = \frac{\pi}{2}\,\theta_R\,\theta_P\,\beta'_{UU}(0)\quad (D_2\text{-}D_1) \qquad (67)$$

where θ_R and θ_P are the beamspread of the receiver and projector respectively, and $\beta'_{UU}(0)$ is the unpolarized scattering index at $\Phi = 0$. In deriving this equation the assumptions are made that θ_R and θ_P are small, and that the scattering index is constant over the small range of angles accepted. Theoretical polar scattering curves for spherical particles indicate that the latter assumption is good for particles up to about 20 microns in diameter.

Since $D_2\text{-}D_1$ appears in equation (67), it would seem that long ranges are undesirable. However, by combining equations (65) and (67), it can be shown that the fractional error in σ, due to scatter, is independent of distance:

$$\epsilon_s(\sigma) = \frac{-\pi\,\theta_R\,\theta_P\,\beta'_{UU}(0)}{2\sigma} \qquad (68)$$

Substituting $\theta_R = \theta_P = .008$ and values for $\beta'_{UU}(0)$ and σ based on theoretical curves by Gumprecht, Sung, Chin, and Sliepcevich (Ref. 12), $\epsilon_s(\sigma) = 0.03\%$ for spherical water droplets one micron in diameter. For fog droplets of 7 microns diameter, forward scatter is proportionately higher, and $\epsilon_s(\sigma)$ increases to about 0.5%. It is evident from this analysis that narrow receiver and projector beams are essential.

The fractional error in transmittance, $\epsilon_w(T_{1-2})$, resulting from various other photometric errors is probably independent of the distances employed. Under this assumption, the fractional error in σ from this source is:

$$\epsilon_w(\sigma) = \frac{\epsilon_w(T_{1-2})}{(D_2-D_1)\,\sigma} \qquad (69)$$

Thus, the conclusion is reached that D_2 should be as large as possible for maximum over-all accuracy.

D. Results of Measurements

The two instruments described above were used to measure a large number of natural fogs, mostly in the Ann Arbor area, and some artificially generated fogs. Figures 9 and 10 show the station wagon which has been specially equipped to transport the instruments.

In many instances the fog was of such short duration that the measurements could not be completed; in others the fog was not sufficiently stable from moment to moment to permit reliable measurements to be made; and in still others equipment failures occurred. Thus, the results presented here represent a relatively small percentage of the total number of fog tests. Many improvements have now been made on the equipment to improve its reliability, accuracy and versatility, and measurement techniques have been perfected to increase materially the likelihood of obtaining useable results on each test.

On the accompanying Polar Scattering Diagrams, the amount of forward scattered light is indicated by the height of the curve at its left end, i.e., at small scattering angles. The amount of back scattered light (back toward the light source) is shown on the right, near $\Phi = 180$ degrees. For the curves labelled H-H, both the projector and the receiver contained polarizers with their polarization axes horizontal (or, more generally speaking, with their polarization axes parallel to the scattering plane.) For the curves labelled VV, both polarizers were vertical, or perpendicular to the scattering plane. For those labelled C (for "crossed"), the projector polarizer was horizontal and the receiver polarizer vertical, corresponding to the designation H-V. The same result

would have been obtained if the polarizers had been in the V-H position.

1. First Test: Artificial Fog, Ann Arbor, July 3, 1956 (Fig. 11)

A small room in Mason Hall at the University was sealed off from all ventilation and filled with steam by running hot tap water for over an hour.

2. Second Test: Natural Fog, Ann Arbor, July 21, 1956 (Fig. 12)

It was estimated visually that the meteorological range was about 1000 feet in this fog. By integration of the Polar Scattering Diagram according to equation (6), it computed to be 811 feet, assuming that the absorption coefficient was negligible.

3. Third Test: Artificial Fog, Pennsylvania State University, Aug. 31, 1956 (Fig. 13)

Both instruments were used to measure a very dense nozzle fog generated by Professor Marsh in a concrete and canvas enclosure. According to the Transmissometer, the meteorological range was 5.8 feet. According to β' integration it was 4.9 feet, and according to visual estimate it was about 5 feet.

4. Fourth Test: Natural Fog, Asbury Park, New Jersey, Sept. 1, 1956 (Fig. 14)

This was an unusually wet fog, with some precipitation present. By β' integration the meteorological range was 1490 feet.

5. Fifth Test: Natural Fog, Ann Arbor, Nov. 2, 1956 (Fig. 15)

This was an unusually homogeneous fog of long persistence. Usually each curve reported is derived from the average of two or three recordings taken under the same conditions, but on this occasion each curve shown is the average of from six to twelve, except one, which is the average of two. The HH and VV curves labelled (a) were taken first. Then the Transmissometer was used to measure small angle forward scatter by the method described above. Some two hours later the main part of the HH and VV curves were measured again (letter b). The reproducibility of curve shapes is seen to be excellent.

6. Sixth Test: Natural Fog, Ann Arbor, Feb. 26, 1957 (Fig. 16)

By β' integration the meteorological range was 1670 feet. There is an infinite number of types of polarizers which could be employed in

both the projector and the receiver.* Previous measurements were made with the three combinations which are of most importance, but on February 26, three additional polarizer combinations were used. From these six, as pointed out above, it is possible to predict the results if any other polarizer combination were employed.

Of particular interest is the fact that no extinction occurs in back scatter, if both the linear polarizer and the linear analyzer are crossed with each other but with both at 45 degrees to the scattering plane, i.e., the DD curve. (This result suggests that if polarized vehicle fog lights are used, they should be polarized either parallel to or perpendicular to the scattering plane. It is also evident from these curves that crossed linear polarizers when properly used are more effective in reducing scattered light than crossed circular or elliptical polarizers.)

7. General Comments on the Measurement Results

Probably the two most surprising aspects of these curves are: (a) the extremely large forward scatter; and (b) the lack of complete extinction under crossed polarizer conditions, particularly in back scatter. During the integration to obtain the scattering coefficient ($b = 2.34 \times 10^{-3}$ ft.$^{-1}$) it was found that the first two degrees contribute about 18% of the integral and the first 20 degrees contribute 56% of the total. It is thus apparent that small angle scattering must be included whether the integration is performed computationally from the scattering curve, or optically, as in an integrating sphere or haze-meter.

Perrin's theory, described earlier in this article, predicts that extinction in direct back scatter will occur for the HV, DD, and RR curves. Although very large angle measurements have not yet been made quantitatively, there does not seem to be any tendency for these curves to approach zero in the case of fog. Visual observations at angles near 180° indicate that the scattered light is essentially unpolarized when the incident light is either circularly or diagonally polarized. Measurements made on a single glass sphere yield similar results, suggesting that multiple scattering is not the cause of the depolarization. Further studies of diffraction theory are evidently necessary to explain this important difference between the clear air and the fog polarization matrices near back scatter.

All of the polar scattering diagrams obtained to date are similar except in over-all height. Thus we may conclude that except for the obviously large differences in density, most if not all fogs, both natural and those artificially-produced from water, have similar light-scattering properties. They all exhibit extremely high forward scatter and minimum scatter at an angle of about 100 degrees. Furthermore, all of the VV curves show a large peak at 140 degrees. This is visible as a large

*The curve for unpolarized source and receiver is approximately equal to the average between the HH and the VV curves, as shown by equation (22) above.

ring of light if one stands in a headlight beam and looks away from the light source. It is called the fogbow (first cousin to the rainbow), and is caused by reflection of the light at the second surface of each droplet.

Although the curves are generally similar, some relatively small differences from one curve to another do exist. Some of these differences are not reliable, being caused by variations in fog density occurring during the measurements. Others are the result of minor errors in instrument calibration (these errors have now been eliminated and improvements made in the optical system of the Nephelometer.) And finally, in one instance, it is believed that the fog was so dense (August 31) that multiple scattering caused a slight "smearing" of the curves. In the presence of these anomalous differences from curve to curve, any real differences that may have existed are difficult to detect.

The Polar Scattering Diagrams have proved invaluable in the present studies of highway visibility in fog in the following ways:

(a) As seen in Section III E below, they permit calculation of the visibility of specified targets in fog.

(b) The data already collected demonstrate that the optical properties of many natural fogs are similar, provided that their densities are alike. With varying densities, the shapes of the curves appear to remain essentially unchanged (as plotted on semi-log paper). If these observations are substantiated by further tests, then future tests, calculations, and measurements can be greatly simplified.

(c) It has also been possible to demonstrate that at least some artificially-produced water fogs are optically equivalent to natural fogs.

(d) Inspection of the Diagrams has suggested improved means of lighting the highway to reduce the loss of contrast caused by the fog. (See Section IV following.)

Many other practical applications will undoubtedly be found for them later.

E. Calculations

Following are sample calculations of the visibility of a circular target as seen through fog by the driver of an automobile. The first calculation assumes that the scene is illuminated only by a conventional street light, as shown in Figure 17. The light is 25 feet, the driver's eyes 4.3 feet, above the roadway. The candlepower distribution is taken from the I.E.S. Handbook, page 8-47. No polarizers are assumed and the Polar Scattering Diagram used is that measured on February 26, 1957 (Figure 16).

The luminance of a section of fog Δl in length is equal to:

$$\Delta B_f = \pi \beta' E_o \Delta l \ , \tag{70}$$

where β' is the polar scattering index for unpolarized light. E_o is the illuminance on the fog:

$$E_o = \frac{I_o}{D_o^2} \ , \tag{71}$$

where:

I_o is the intensity of the street light in a given direction.

D_o is the distance from light to fog sample.

The luminance of the fog for each foot of fog along the driver's line of sight is defined as:

$$B'_f = \frac{\Delta B_f}{\Delta l} = \pi \beta' E_o \ , \tag{72}$$

Finally, B_f is defined as the total luminance of the fog from the driver's eye to the target location.

Table I shows these quantities for each ten degree increment in scattering angle Φ.

The dashed curve of Figure 17 shows the luminance per foot of fog (B'_f) in the direction of the driver's eye. Note that it is high at the left because of high forward scatter, with a minimum almost directly under the light.

Figure 18 shows the total luminance, B_f, of the fog between the eye and a target at various distances from the eye, and Figure 19 shows the transmittance of the fog (for image-forming rays) as a function of distance.

As an example of how available visual detection threshold data can be used, let us assume that there is an object on the roadway. The object is circular, 2 feet in diameter at eye level. The target luminance is 0.08 foot-lamberts and the background is .10 foot-lamberts. Since it is 116 feet from the eye, Figure 21 shows that the target and background luminances will be reduced by virtue of the transmittance of the fog to .0615 and .077, respectively. But the fog will add to each of these 0.276 foot-lamberts luminance, bringing their luminances to 0.337 and 0.353, respectively. The contrast is thereby reduced to .045, from an initial value of .200. Now, we examine Figure 1 to ascertain

the contrast required for visual detection with a background of 0.353 foot-lamberts. Log B is -.453. The angular size of the target is 60 minutes. We may read the log contrast from the value of the bottom curve in Figure 1 at a log B of -.453. The value obtained for log contrast is -1.30. This is equal to a contrast of .0503. Since this value is greater than .045, it is apparent that the fog will reduce the target contrast below the amount required for visual detection.

(It should be pointed out that the data presented in Figure 1 are laboratory data, representing a detection probability of only 50%. We can be certain that the target will not be visible any appreciable percentage of the time in a practical field situation, where visual detection is known to be more difficult.)

The calculational method has not as yet been used in any practical way. The sample calculations presented above were performed only to demonstrate that calculations can be made relatively easily, provided that certain simplifying assumptions are made, for example that the effect of doubly scattered light is negligible. It is believed that the method will be valuable later in optimizing the design of light source characteristics, retro-reflector properties, etc., to enhance visibility through fog.

The studies of the optical properties of the atmosphere, and the calculations reported in this section represent the portions of the joint Michigan-Pennsylvania State Fog Visibility Program which we were committed to conduct. These studies do represent our major effort and, thus, this section could serve as a final report of our activities under the IERI grant. However, toward the end of the grant period, we undertook several additional minor activities which are reported in the sections following.

IV. PRELIMINARY SUGGESTIONS FOR IMPROVED HIGHWAY ILLUMINATION FOR USE IN FOG

The Polar Scattering Diagrams exhibited in Section III above were studied by our staff, by Prof. Marsh, and by Mr. C. L. Crouch, Secretary of the IERI. The curves for H-H and V-V exhibit a characteristic of considerable importance for the design of street lights. It is apparent from the curves that the magnitude of scatter is much less for angles from 70° to 130° than for angles either greater or less. This means that street light illumination at angles far from direct down-light contributes a great amount of scattered light in the direction of the driver's eye. This light scatter produces a light veil of considerable luminance, which reduces the contrast of a truck, for example, against the roadway and the contrast of the truck taillights against the truck.

It occurred to us, to Mr. Crouch and to Prof. Marsh that elimination of the light rays emanating from the street light at extreme angles would reduce the light veil and should increase visibility. Oversimplification of the problem must be avoided. Obviously, although narrowing the beam of the street lights will reduce the light veil, it will also reduce the illumination falling upon the truck and roadway, with possible reduction in their visibility. Of course, introduction of additional street lights with narrow-beam "down light" should compensate for this loss in illumination. Perhaps the most effective system would involve narrow-beam street lights directed some 10° forward from vertical. These beams would produce increased illumination on vertical surfaces such as the back of the truck, and would take advantage of the fact that the minima of the polar scattering diagrams are at 100°.

A second obvious characteristic of the curves is the great reduction in the light scatter for the H-V and V-H cases, with respect to the H-H and V-V cases. This suggests that street lights might well be linearly polarized, and the scene viewed through an analyzer of opposite polarization. Such a system would be expected to reduce the light veil greatly. However, here again the problem must not be oversimplified. The use of polarized street lights reduces the illumination on objects and the roadway, unless the intensity of the street light is increased to compensate. Furthermore, there are objects on the highway which are usually seen by specular reflection, such as shiny bumpers, glossy paint, etc. In many cases, the use of a polarized viewing screen will eliminate the specular "glints" characteristic of these objects.

These two suggestions for modifications in street lights for use in fog were evaluated by Prof. Marsh in his scale-model simulator. Marsh found that, in each case, the light veil was considerably reduced, as expected. In each case, there appeared to be a significant improvement in the visibility of objects on the highway. We at Michigan also evaluated these ideas in a scale-model simulator (see Section V below) and confirmed Marsh's conclusions.

It must be emphasized that these suggestions for improving visibility on the highway do not necessarily take into consideration all the complex variables involved in seeing to drive safely through fog. It is necessary to begin any comprehensive evaluation of improved techniques for seeing through fog by specifying the visual tasks required of the driver. For example, it may not be possible to render the roadway and all objects on it visible. It may have to suffice to render major obstacles sufficiently visible to avoid collisions, and to render the roadway sufficiently visible to enable the driver to stay on the road. Once the visual tasks are specified, techniques may be evaluated in terms of their effect upon the performance of these tasks. Furthermore, care must be taken to insure that various techniques are evaluated under the range of conditions of practical interest. For example, the effectiveness of a polarized system may be expected to depend upon the polarization characteristics of materials used in automobiles, roadway markings, and roadway signs.

Thus, the two specific suggestions of methods for improving the effectiveness of street lights for use in fog must be regarded as preliminary notions, based upon the simplest interpretation of the significance of the Polar Scatter Diagrams. Quantitative evaluation of these ideas must be undertaken before they can be given serious consideration for practical use. The final evaluation of these, and other ideas, will have to be accomplished in a further research program, because the funds for the present program are currently exhausted.

It seems apparent that evaluation of the effectiveness of various methods of improving visibility on the highway in fog must be performed in the "total environment" of the problem, to the maximum possible extent. We believe that scale-model simulation has an important use in such evaluations, (see Section V below). Of course, full-scale field test and evaluation must be used as the final criterion of the effectiveness of a system.

V. DEVELOPMENT OF A SCALE-MODEL SIMULATOR AND PRELIMINARY OBSERVATIONS IN IT

Upon learning that Prof. Marsh was evaluating the suggestions for improved street lights (see Section IV above) in his scale-model simulator, we assembled components to produce scale-model simulation for our study. Scale-model cars were equipped with headlights and taillights, miniature street lights were constructed, and a room in the basement of Mason Hall at the University was filled with fog using a nozzle provided by Prof. Marsh. The model simulator was easy to construct and manipulate, and seemed most useful. Preliminary observations were made to assess the effectiveness of narrow-beam street lights, and polarized street lights. Both these suggestions seemed sufficiently promising to merit further consideration. It was not possible to continue using this simulator, however, since building inspection rules prevented further use of the room for this purpose. Consequently, a few days before the scheduled "Visibility in Fog Demonstration" at the Pennsylvania State University, a "fog box" scale-model simulator was constructed as shown in Figure 22.

A. Requirements of a Simulator

It can be shown that in a model simulator of scale s (in the present fog box, s = 25), all luminances, illuminaces, and contrasts seen by an observer looking into the simulator will be exactly equal to the corresponding quantities in the full-scale situation, provided the following conditions are fulfilled:

(a) All linear dimensions of automobiles, roadways, etc. are reduced by the scale factor s. Thus,

$$D' = \frac{1}{s} D \qquad (73)$$

where D is the dimension of an object in the full-scale scene, and D' is the dimension of its scaled-down counterpart in the simulator.

(b) The candlepower of all light sources should be reduced by the square of the scale factor:

$$I' = \frac{1}{s^2} I \tag{74}$$

(For example, if the full-scale street light has an intensity of 5,000 candles in a particular direction, the corresponding intensity in the 25-to-1 simulator would be 8 candles. The large and the small lights would then produce the same level of illumination on the street surfaces below them.)

(c) The fog in the simulator should be denser than the full-scale fog being simulated by the scale factor:

$$\sigma' = s\sigma \tag{75}$$

$$(\beta')' = s\,\beta' \tag{76}$$

Also, the meteorological range (often incorrectly called "the visibility") in the simulator should be reduced by the scale factor:

$$V' = \frac{1}{s} V \tag{77}$$

(d) All reflectances should remain unchanged. Thus ordinary paints, reflectors, and retro-reflective materials are directly useable in the simulator.

$$R' = R \tag{78}$$

To monitor the density of the fog in the simulator, the Portable Transmissometer described above was employed, looking through two holes in the fog box as shown in Figure 22. With no fog in the box, filters were introduced and the sensitivity adjusted until the meter read 100%. From equations already presented, it is possible to determine the relationship between the meter reading when the fog is introduced, the meteorological range in the box, and the meteorological range in the corresponding full-scale situation. The fog path length is approximately equal to the width of the box, two feet. From equation (2),

$$T' = {}^{-\sigma' x 2} \tag{79}$$

from which

$$\sigma' = -1/2 \ln T' \tag{80}$$

Now, from equation (3),

$$V' = \frac{3.912}{\sigma'} = \frac{-7.824}{\ln T'} \tag{81}$$

For example, when the Transmissometer indicates a transmittance of 14%, the meteorological range V' in the simulator is four feet, which corresponds according to equation (77) to a full-scale fog of 100 feet meteorological range.

B. Observations in the Simulator

In addition to evaluation of the narrow-beam and polarized street light conceptions, the scale-model simulator has been used for preliminary evaluation of different headlamps, tail lamps and roadway marker systems. Several suggestions have emerged from these preliminary evaluations.

Vehicle headlights should be mounted as low as possible in order to reduce the illuminance on the fog in the driver's line of sight, and they should probably be "cross-eyed" to illuminate the guide lines on the roadway.

The most effective way to make a target visible is to make it self-luminous rather than to attempt to illuminate it. Auxiliary taillights for use in fog should therefore be employed with greatly increased candlepower. Narrow-beam street lights, cross-eyed low-mounted fog lights, and taillights of increased candlepower seem to constitute the best combination we have evaluated to date. All these features were set up in the scale-model simulator, and the photograph was taken which is exhibited as Figure 23. For comparison, a photograph was taken seconds later in the scale-model simulator with the present type headlights, taillights and wide-beam street lights in use. This photograph is exhibited in Figure 24. There is a clearly perceptible improvement in the visibility of the automobile in the driver's lane in Figure 23, in comparison with Figure 24. The difference evident in the photographs was even more obvious to each observer asked to compare the two conditions under test. These tests, and the photographs obtained in the scale-model simulator

indicate the value of this device in further study of the highway fog problem.

Although it has not yet been demonstrated, we believe that small low-mounted lights along the roadway which direct a narrow beam of light back toward the oncoming traffic would be most effective in demarcating the highway, just as airport runway lights show the location of the strip without actually illuminating it. Such a system might be the only possible system for use in the most dense fog. It might be practical to install such a system on a portion of the roadway where serious fog is to be expected frequently.

It should be emphasized that we do not pretend to have discovered the "solution" to the serious problem of visibility on the highway in fog. However, the ground work has been carefully laid, as there is now a thorough understanding of the physics of the problem, instrumentation has been developed with which to measure the important variables, and techniques have been developed by which suggested improvements in street lights, vehicle lights, or roadway markers can be evaluated quickly and accurately. We believe further research into the problem of visibility through fog, along the lines indicated by this report, would be most fruitful.

REFERENCES

Number	Title	Page
1	Blackwell, H. R., I.E., 57, 602 (1952).	1
2	Middleton, W. E. K., Vision Through the Atmosphere, Univ. of Toronto Press (1952).	2
3	Perrin, F., J. Chem. Phy., 10, 415 (1942).	3
4	Jones, R. Clark, J. Opt. Soc. Am., 37, 107 (1947).	4
5	Billings, B. H. and Land, E. H., J. Opt. Soc. Am., 38, 819 (1948).	4
6	Stokes, G. G., Trans. Camb. Phil. Soc., 9, 399 (1852).	4
7	Waldram, J. M., Trans. Illum. Eng. Soc., London, 10, 147 (1945).	
8	Billings, B. H., J. Opt. Soc. Am., 41, 966 (1951).	9
9	Pritchard, B. S. and Trytten, G. W., J. Opt. Soc. Am., 47, 118 (1957).	17
10	Foitzik, L., Wiss. Abh. Reichsamt f. Wetterdienst, Berlin, 4, No. 5 (1938).	18
11	Stewart, H. S. and Curcio, J. A., J. Opt. Soc. Am., 42, 801 (1952).	18
12	Gumprecht, Sung, Chin, and Sliepcevich, J. Opt. Soc. Am., 42, 226 (1952).	

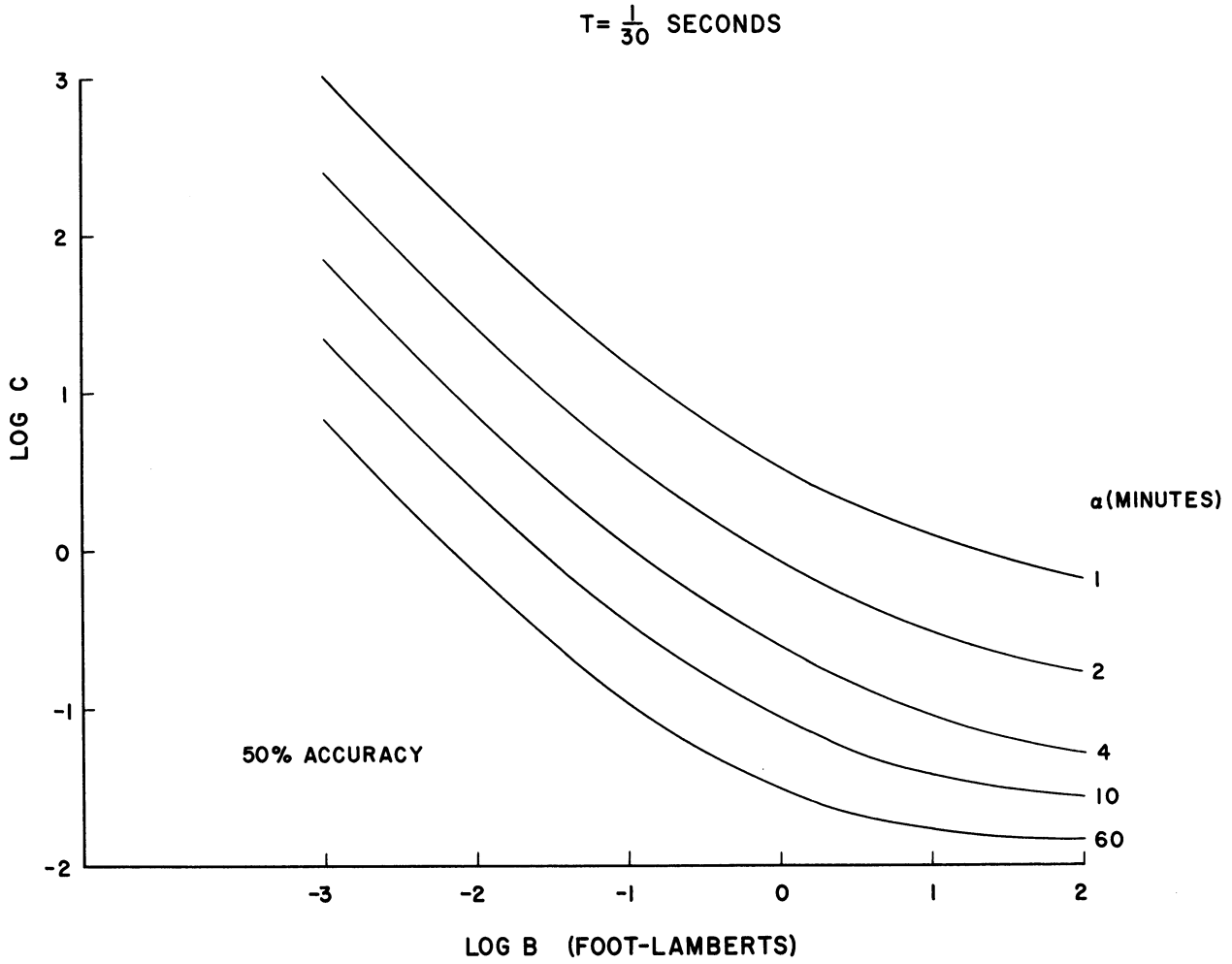

Fig. 1. Threshold contrast as a function of background luminance for circular targets of various sizes. Target exposure duration 1/30 second.

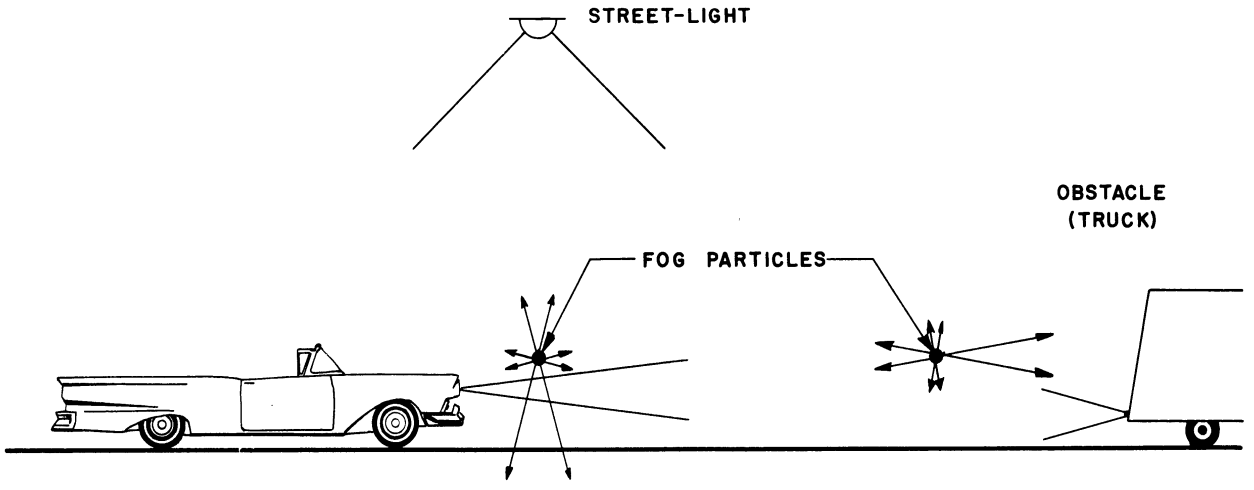

Fig. 2. Artist's conception of the highway visibility situation in fog. The fog particle shown at the left is illuminated principally by the street light, the one at the right by the car headlights. Each scatters light in all directions as shown by the arrows, thus obscuring the truck ahead.

Fig. 3. Recording Polar Nephelometer. This instrument is used to measure the light scattering properties of fog.

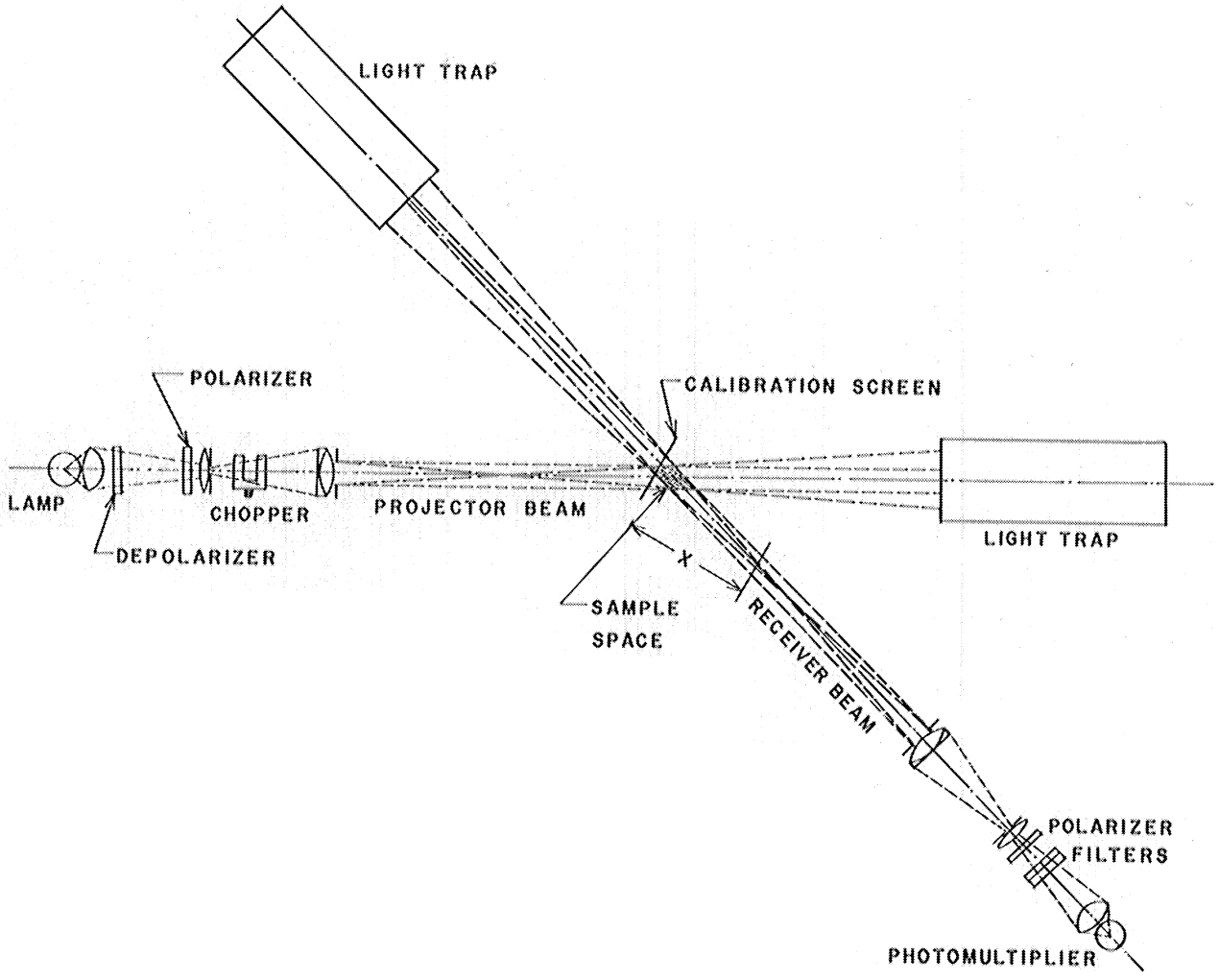

Fig. 4. Recording Polar Nephelometer Optical Schematic.

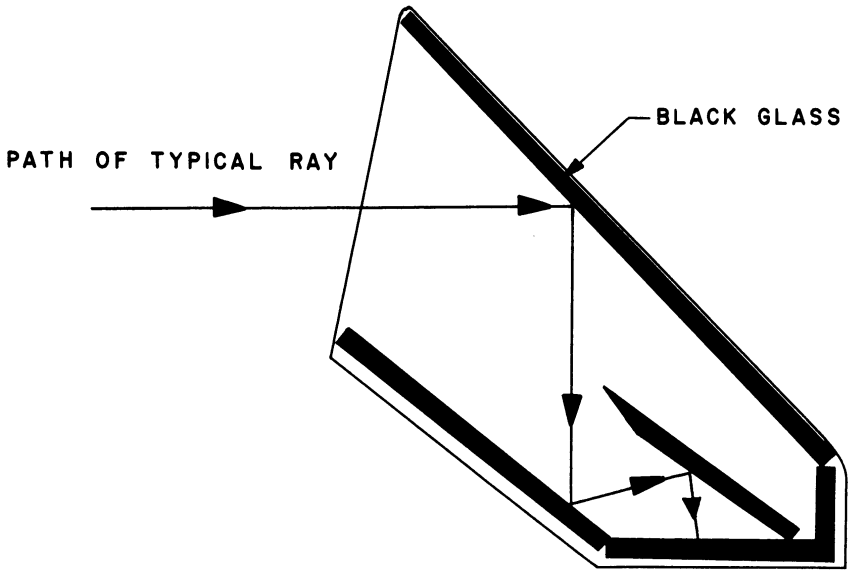

Fig. 5. Recording Polar Nephelometer Light Trap.

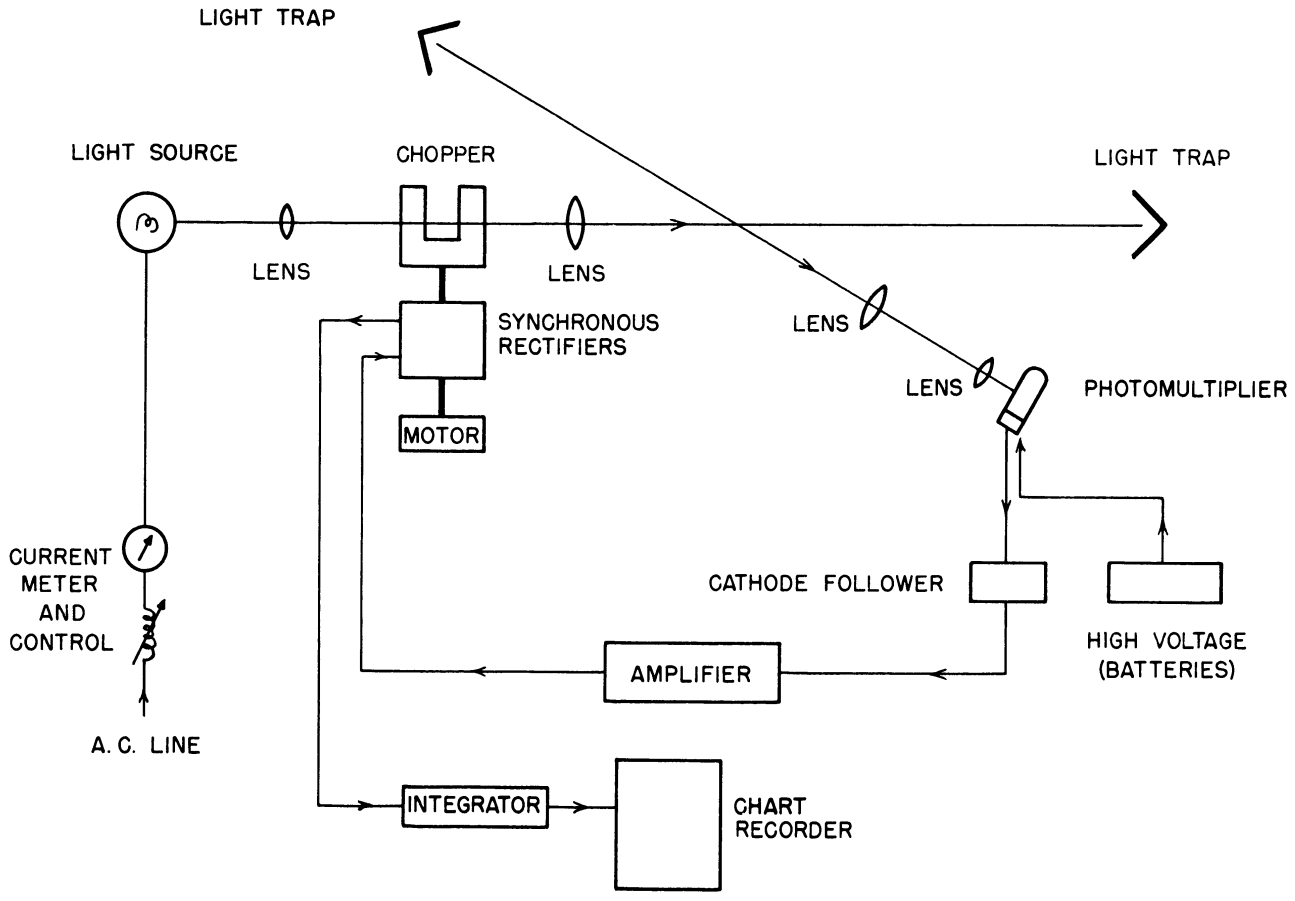

Fig. 6. Recording Polar Nephelometer Block Diagram.

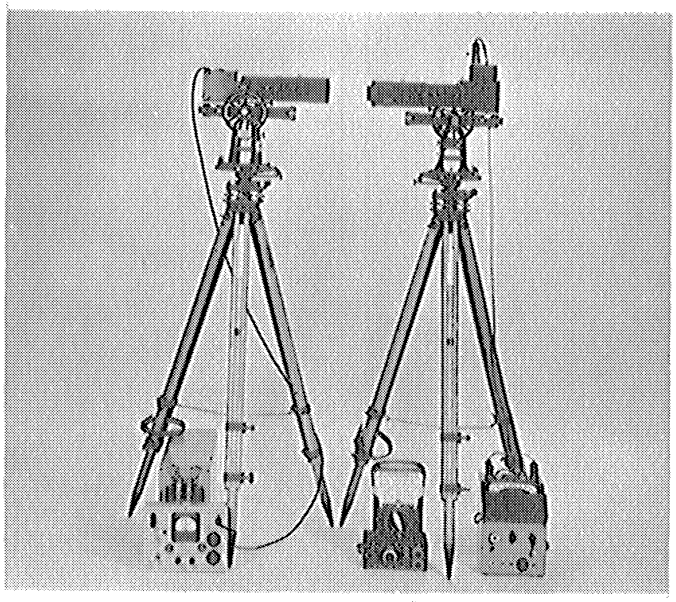

Fig. 7. Portable Transmissometer. This instrument is used to measure the light transmission properties of fog.

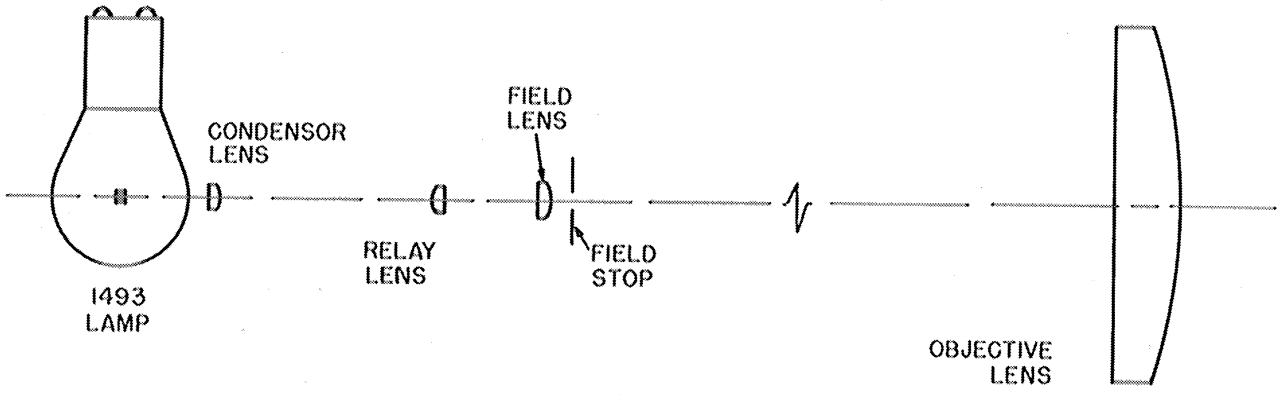

Fig. 8. Portable Transmissometer Projector Optical Schematic.

Fig. 9. The Mobile Receiving Unit. The Recording Polar Nephelometer and Portable Transmissometer are transported to the measurement site in a modified station wagon. A gasoline driven generator in the trailer furnishes electrical power for the instruments.

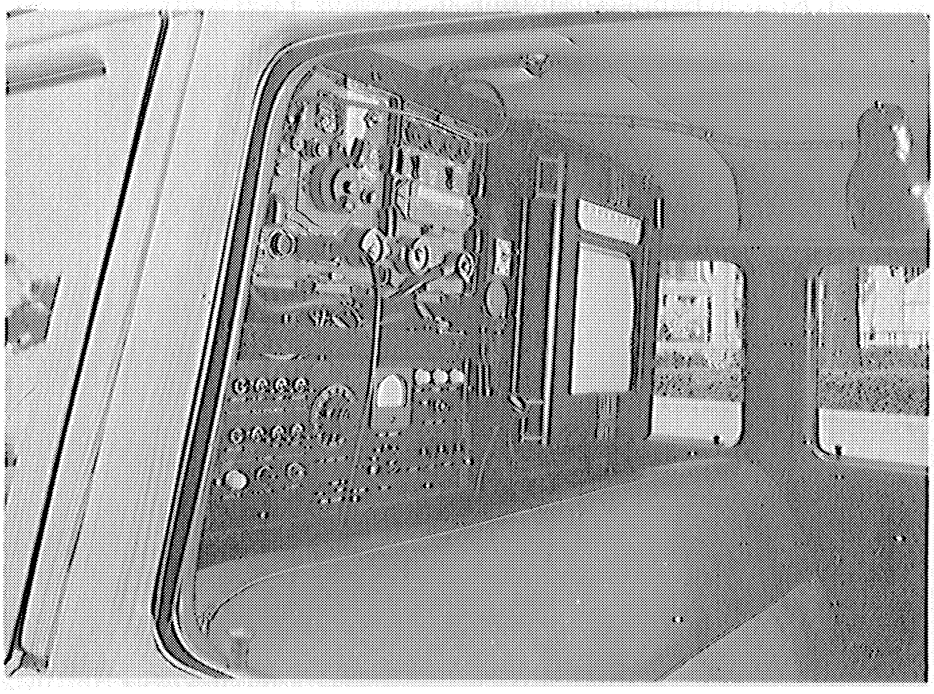

Fig. 10. Interior of Station Wagon. An F.M. Transceiver (upper left), controls for all the Polar Nephelometer (lower left), and the recorder (right) are mounted behind the front seat of the station wagon.

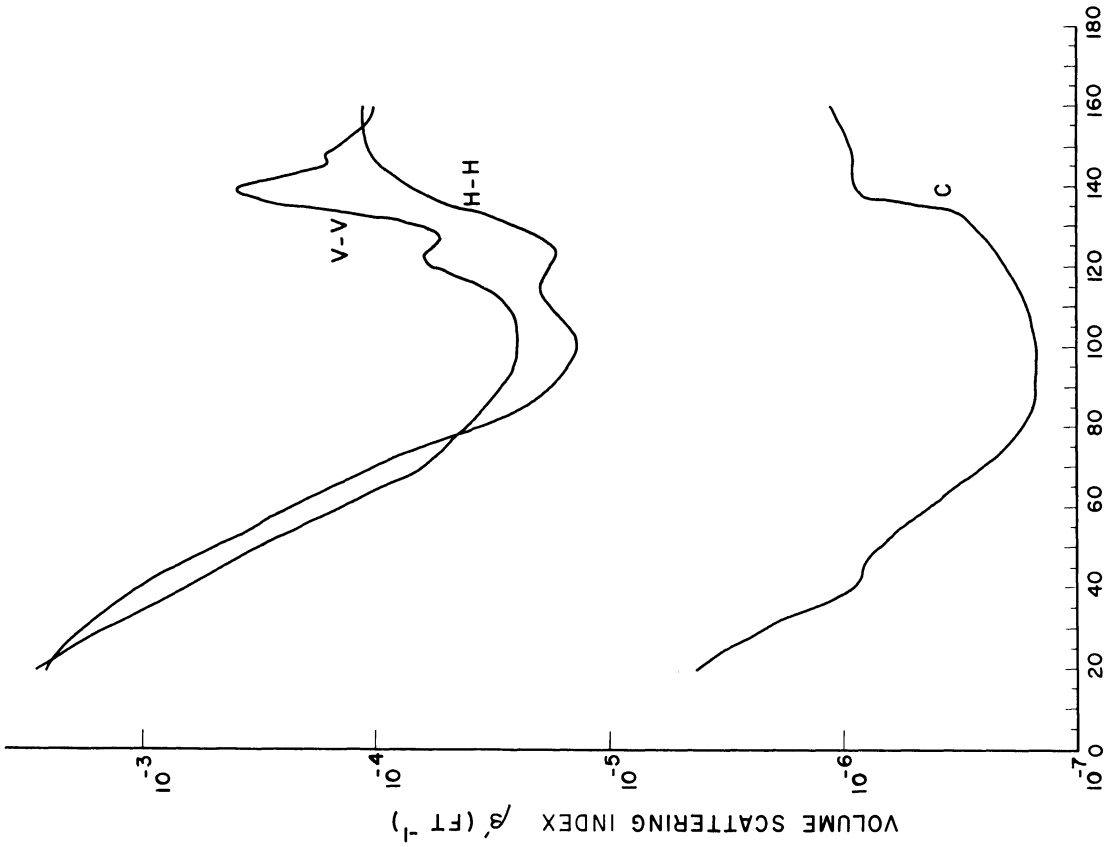

Fig. 12. Polar Scattering Diagram: natural fog, Ann Arbor, July 21, 1956.

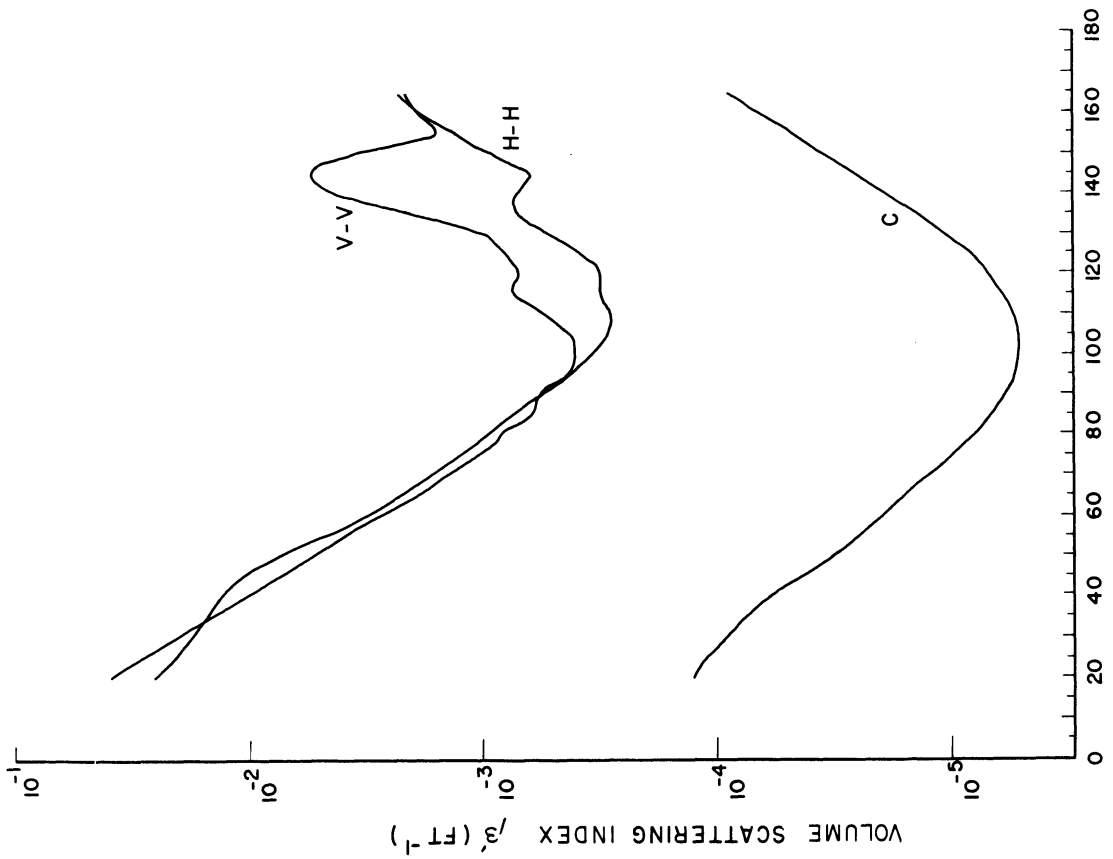

Fig. 11. Polar Scattering Diagram: steam fog, Ann Arbor, July 3, 1956.

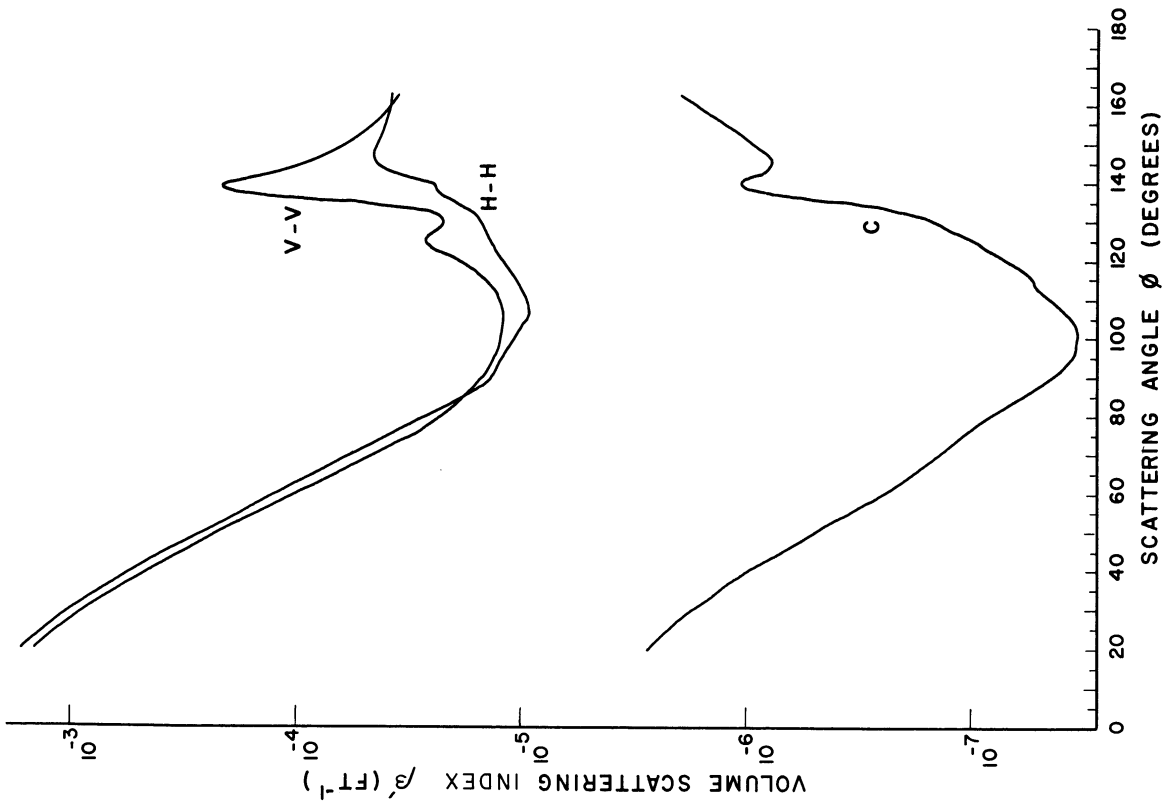

Fig. 14. Polar Scattering Diagram: natural fog, Asbury Park, New Jersey, September 1, 1956.

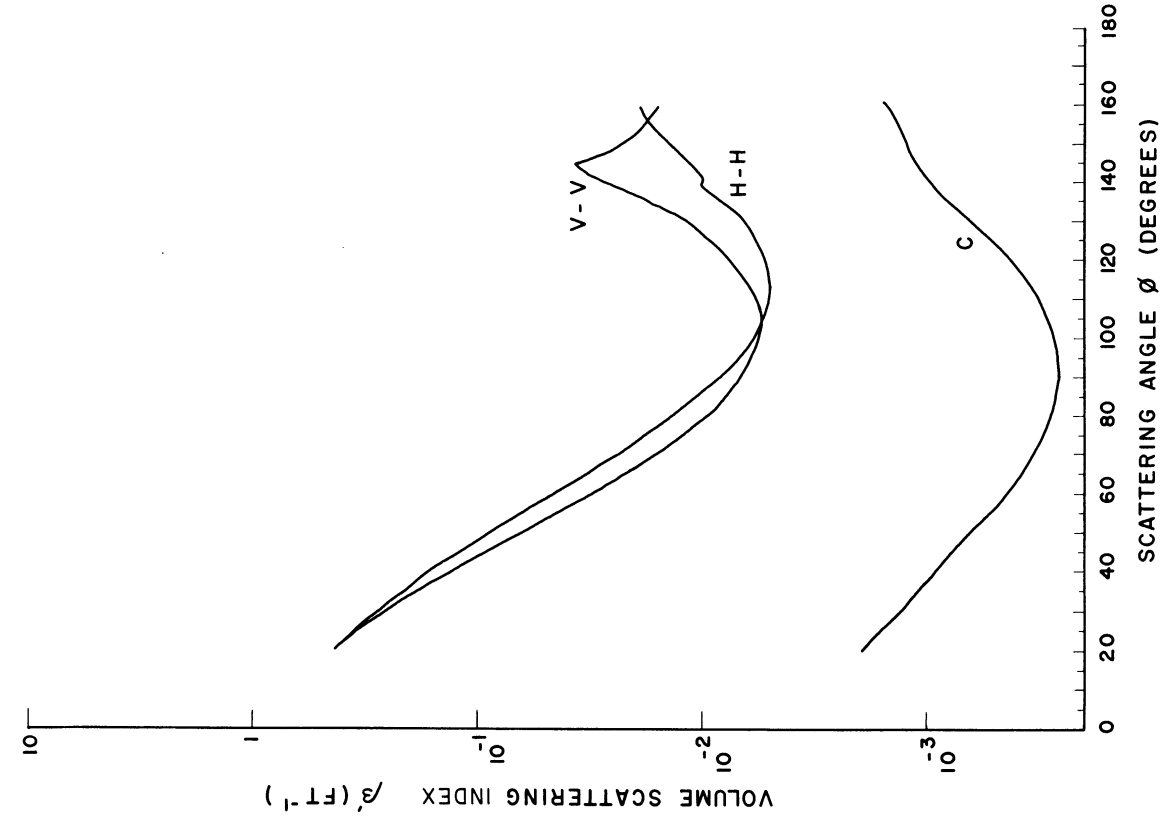

Fig. 13. Polar Scattering Diagram: fog produced by nozzle at Pennsylvania State University, August 31, 1956.

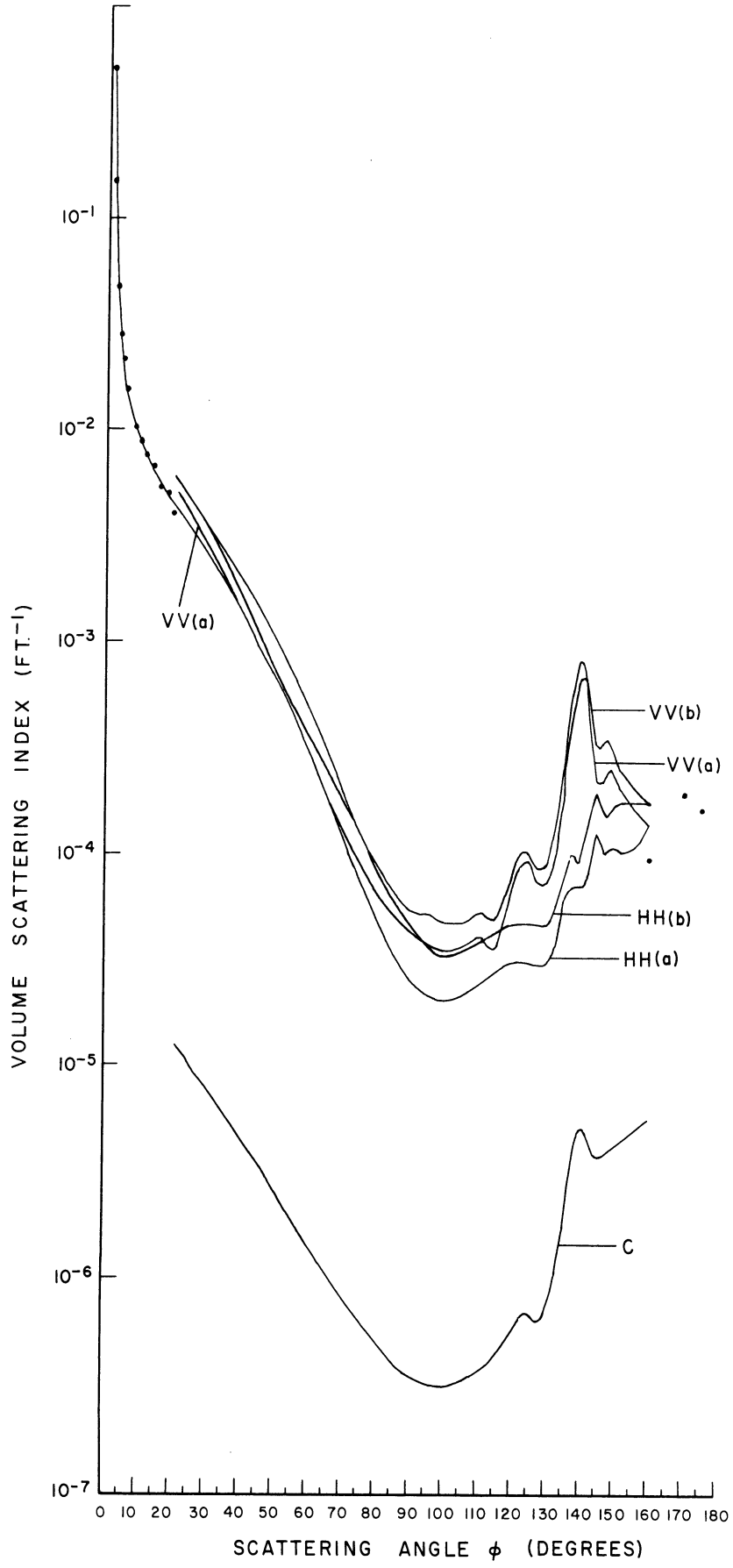

Fig. 15. Polar Scattering Diagram: natural fog, Ann Arbor, November 2, 1956.

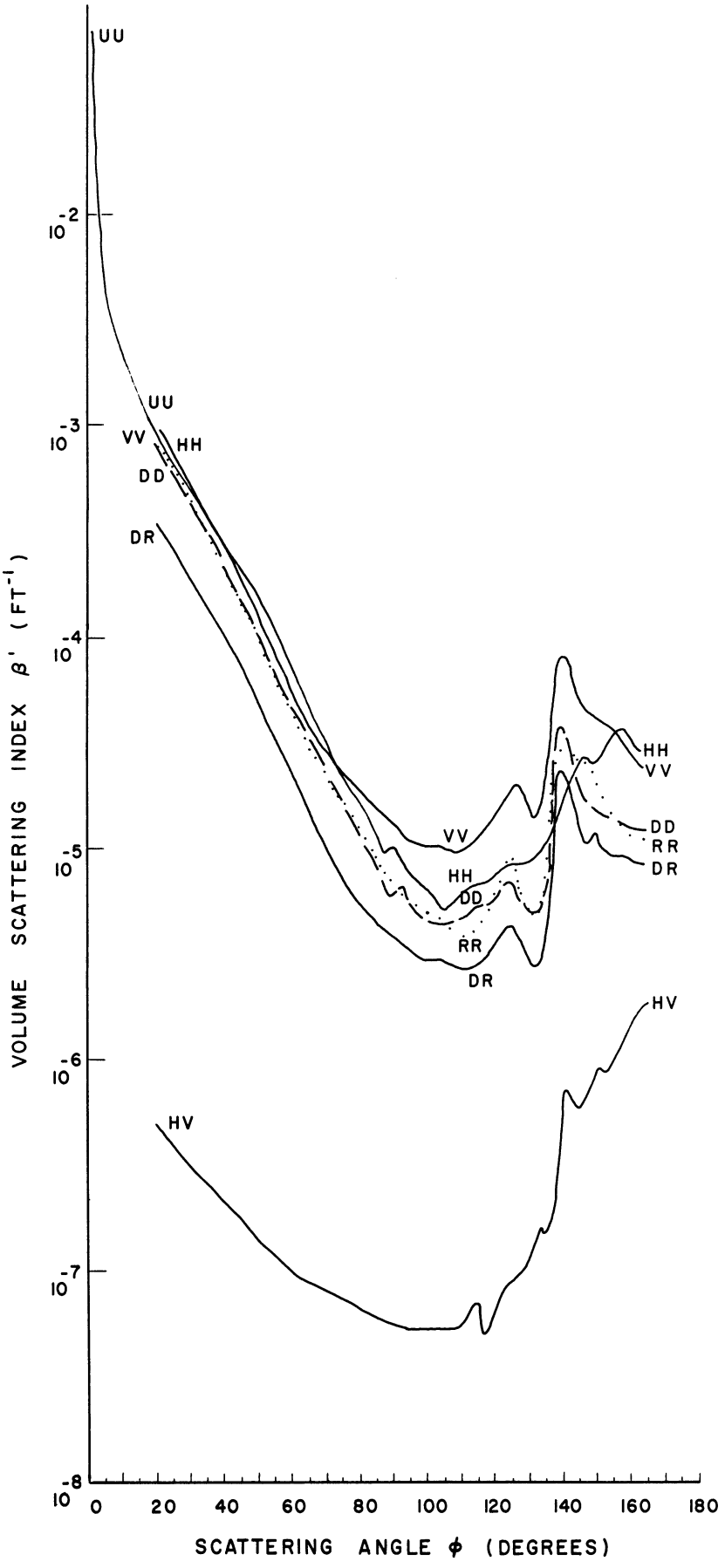

Fig. 16. Polar Scattering Diagram: natural fog, Ann Arbor, February 26, 1957.

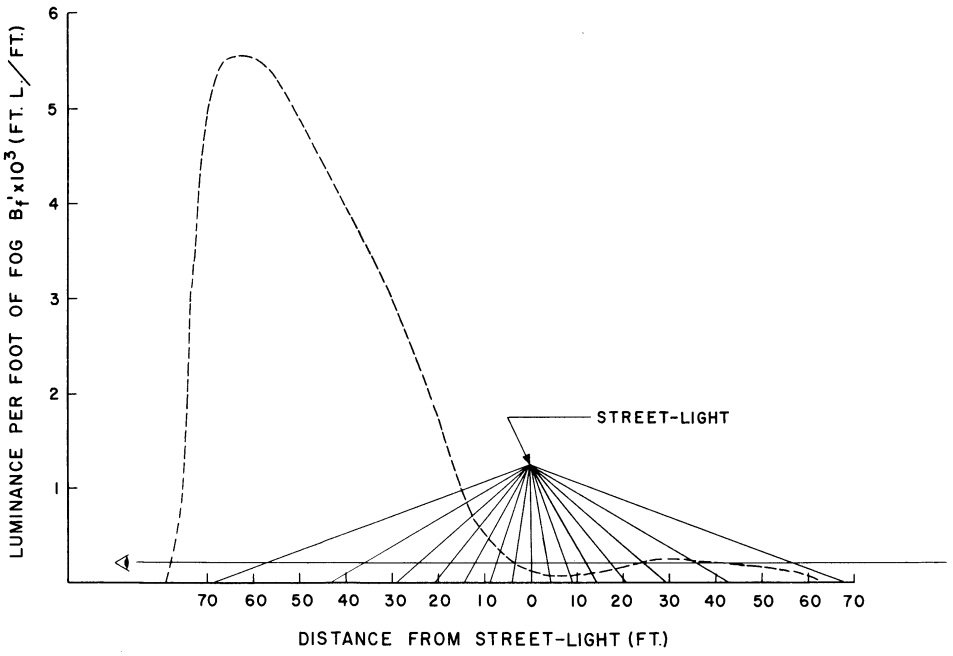

Fig. 17. Luminance per foot of fog under a typical street light. Each foot of fog along the driver's horizontal line of sight adds to the light veil. The amount added in foot-Lamberts is plotted on the vertical axis as a function of the position under the street light, on the horizontal axis.

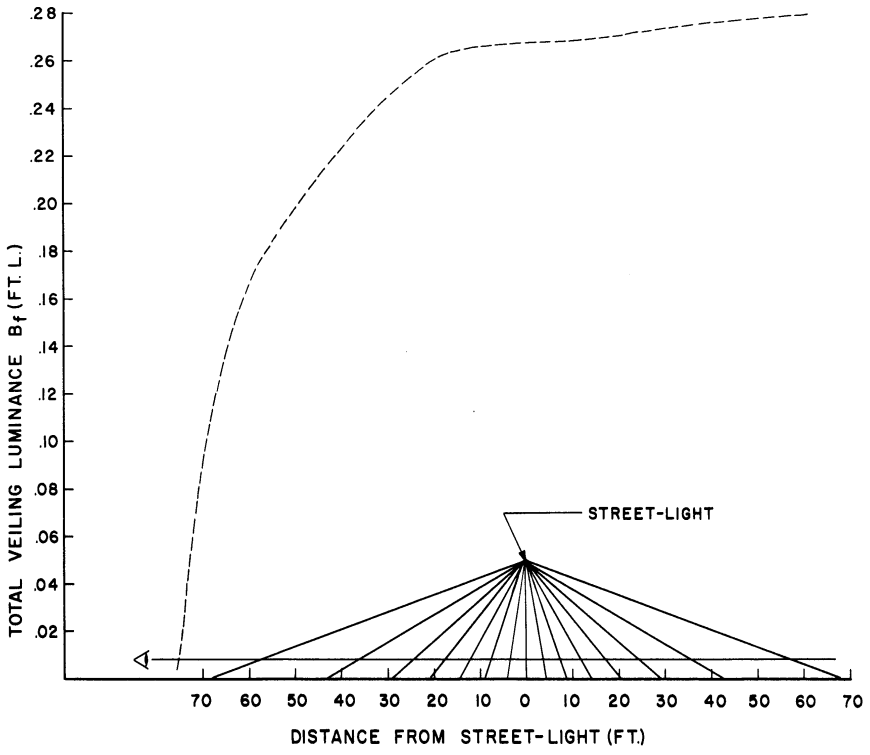

Fig. 18. Total luminance of fog under street light, obtained by integration of the curve of Fig. 17. The driver is assumed to be located just outside the area illuminated by the street light, as shown at the left. The object he is looking for is located under the street light in various locations as indicated on the horizontal axis. The total light veil for each target location is indicated on the vertical axis.

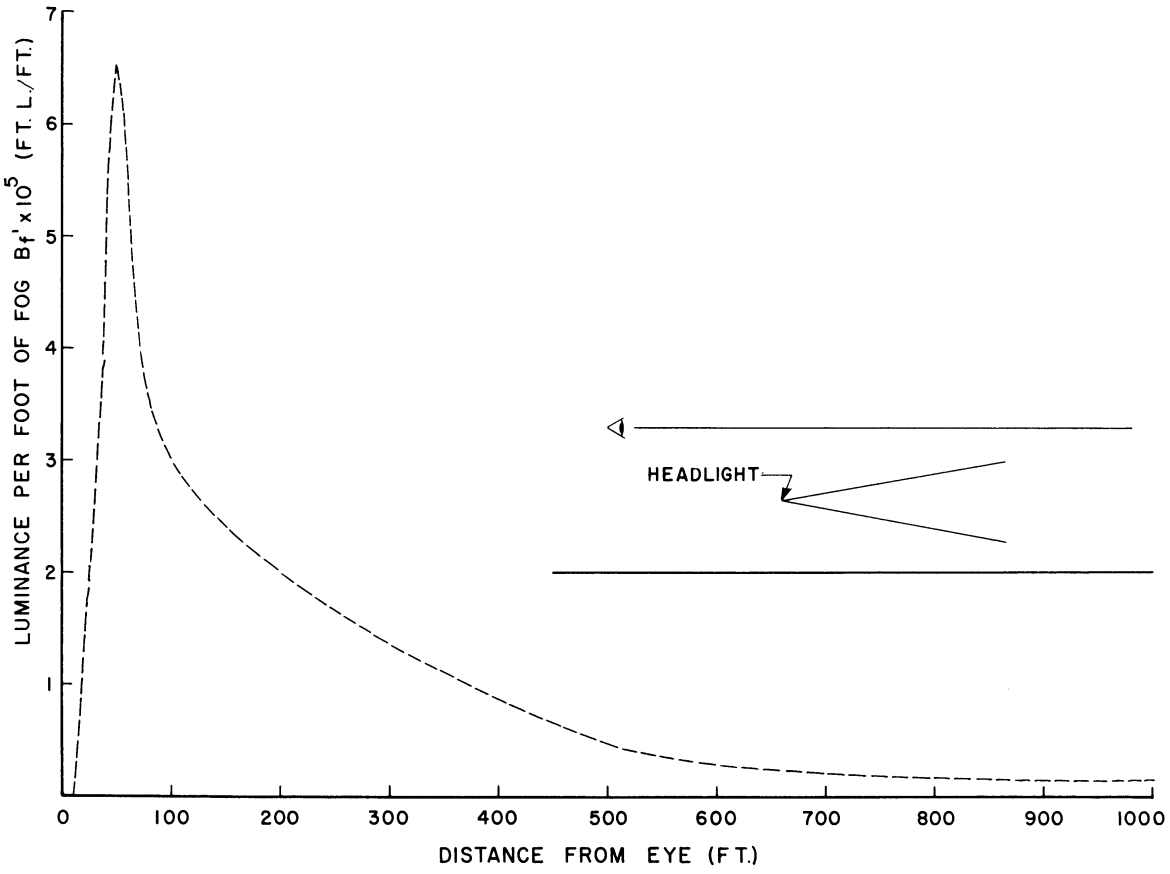

Fig. 19. Luminance per foot of fog under headlight illumination.

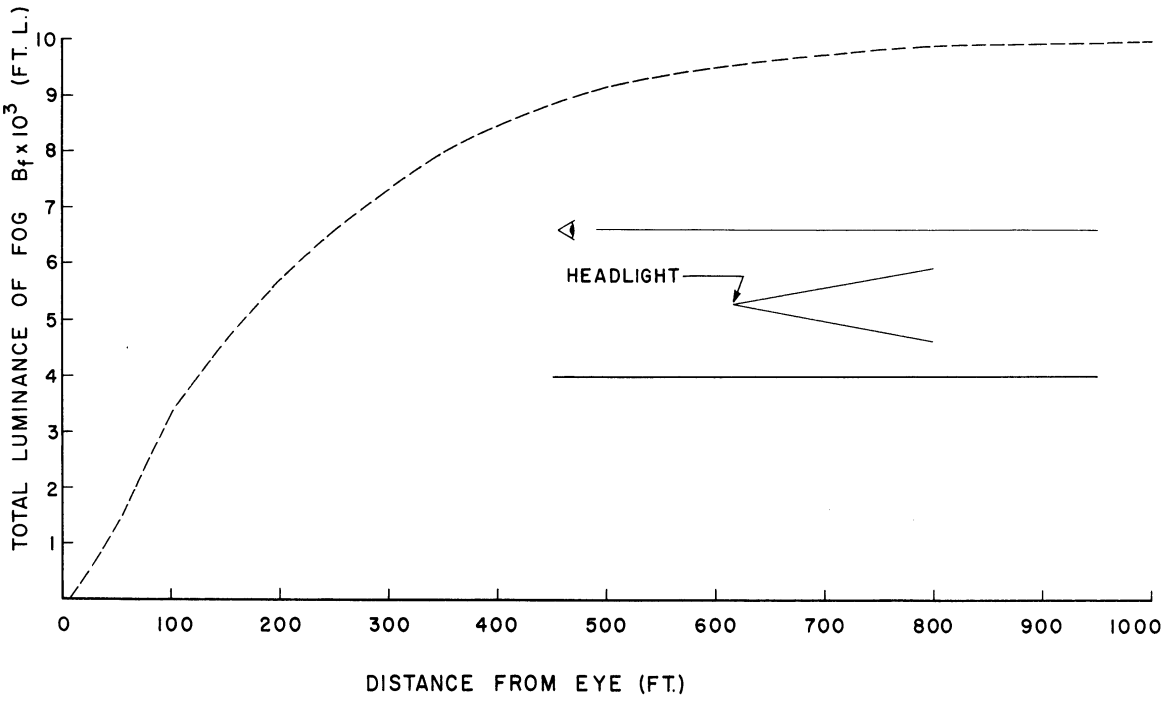

Fig. 20. Total luminance of fog under headlight illumination for variable object location.

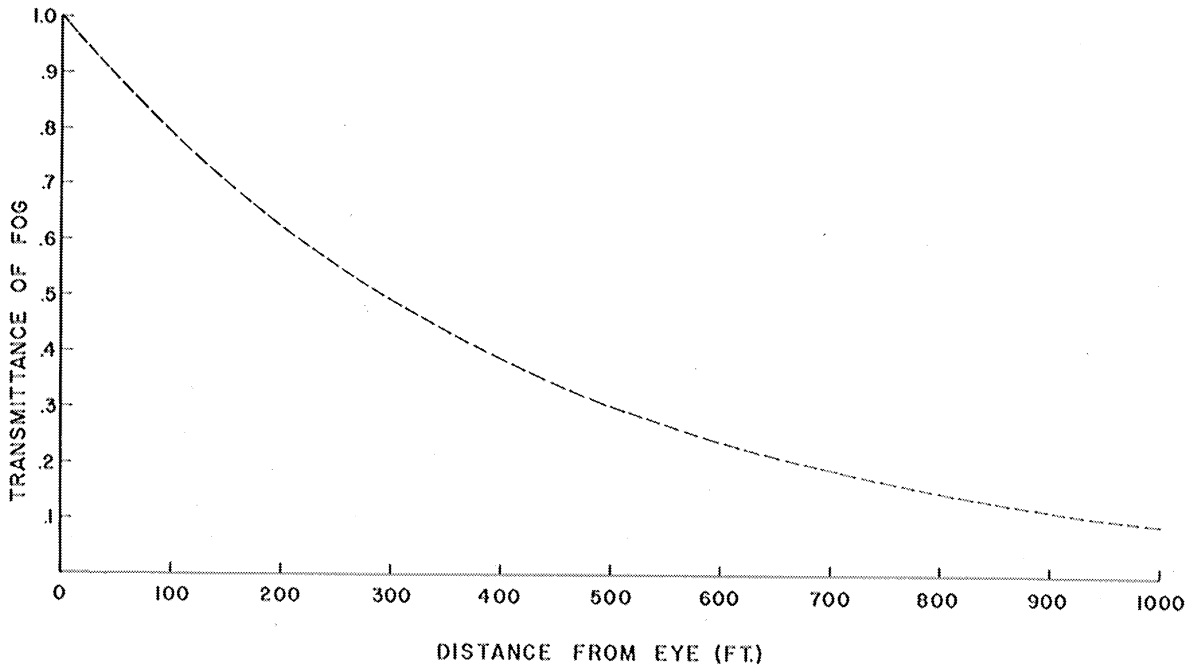

Fig. 21. Transmittance of fog for various path lengths.

Fig. 22. Scale-model simulator. The sub-model cars and street lights are shown inside the box, which may be filled with artificially produced fog. The "peep hole" through which one obtains a driver's-eye view of the roadway can be seen near the bottom of the near end of the box.

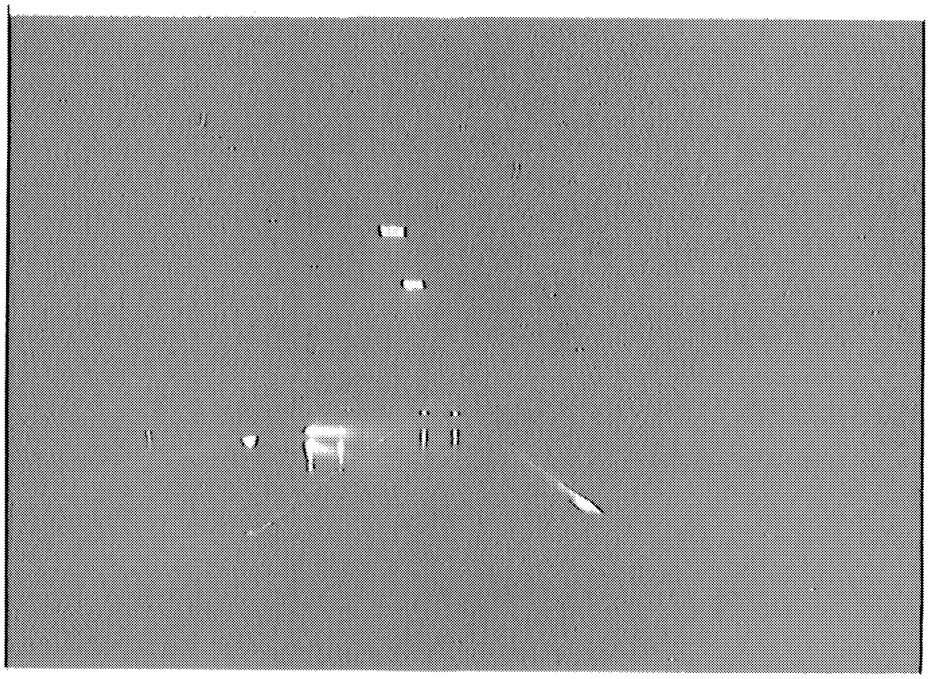

Fig. 23. Improved highway lighting in fog. This photograph was taken through the peep hole in the fog box, with increased candlepower taillights on the car on the right, narrow-beam street lights and "cross-eyed" low-mounted fog lights on the approaching car and the driver's car.

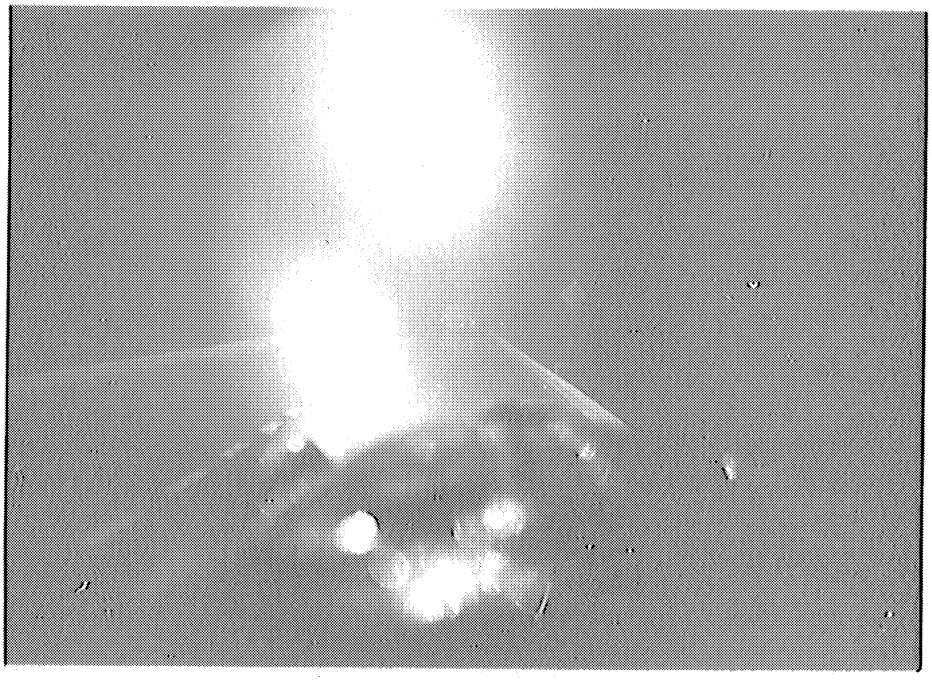

Fig. 24. Normal highway lighting for comparison with previous figure.

TABLE I

Results of Calculations of Veiling Luminance of Fog Illuminated by a Street Light

D (ft.)	Φ (deg.)	I_o (c)	D_o (ft.)	E_o (ft.c)	β' ($ft.^{-1}$)	Δl (ft.)	ΔB_f (ft.L.)	B_f' (ft.L.)	B_f (ft.L.)
57.0	20	5300	60.5	1.45	12.0×10^{-4}	33.0	.180	54.5×10^{-4}	.180
35.8	30	3500	41.4	2.04	5.7	14.7	.054	36.5	.234
24.6	40	2500	32.2	2.41	3.05	8.9	.0205	23.1	.254
17.4	50	2100	27.0	2.88	1.56	6.2	.0088	14.1	.260
12.0	60	1700	23.9	2.98	.71	4.85	.0032	6.65	.266
7.5	70	1600	22.0	3.31	.34	4.10	.0014	3.53	.267
3.6	80	1600	21.0	3.63	.187	3.75	.0008	2.13	.268
0	90	1500	20.7	3.50	.116	3.60	.0005	1.27	.268
-3.6	100	1600	21.0	3.63	.084	3.75	.0004	.96	.269
-7.5	110	1600	22.0	3.31	.082	4.10	.0003	.85	.269
-12.0	120	1700	23.9	2.98	.113	4.85	.0005	1.06	.270
-17.4	130	2100	27.0	2.88	.150	6.21	.0008	1.36	.271
-24.6	140	2500	32.2	2.41	.275	8.90	.0019	2.08	.273
-35.8	150	3500	41.4	2.04	.35	14.70	.0033	2.24	.276
57.0	160	5300	60.5	1.45	.29	33.0	.0043	1.32	.280